

# Measurement Report: Optical Characterization, Seasonality, and Sources of Brown Carbon in Fine Aerosols from Tianjin, North China: Year-round Observations

Zhichao Dong<sup>1</sup>, Chandra Mouli Pavuluri<sup>1\*</sup>, Peisen Li<sup>1</sup>, Zhanjie Xu<sup>1</sup>, Junjun Deng<sup>1</sup>, Xueyan Zhao<sup>1</sup>, Xiaomai Zhao<sup>1</sup>, Pingqing Fu<sup>1</sup>, Cong-Qiang Liu<sup>1</sup>

<sup>1</sup>Institute of Surface-Earth System Science, School of Earth System Science, Tianjin University, Tianjin 300072, China

Correspondence to: Chandra Mouli Pavuluri ([cmpavuluri@tju.edu.cn](mailto:cmpavuluri@tju.edu.cn))

## Abstract

To investigate the optical characteristics and sources of brown carbon (BrC) in North China, where the atmospheric aerosol loadings are high and have severe impacts on the Earth's climate system, we collected fine aerosols (PM<sub>2.5</sub>) at an urban site in Tianjin over a 1-year period. We measured the ultraviolet (UV) light absorption and excitation emission matrix (EEM) fluorescence of the water-soluble BrC (WSBrC) and the water-insoluble but methanol-soluble BrC (WI-MSBrC) in the PM<sub>2.5</sub> using a three-dimensional fluorescence spectrometer. Average light absorption efficiency of both WSBrC ( $Abs_{365, WSBrC}$ ) and WI-MSBrC ( $Abs_{365, WI-MSBrC}$ ) at 365 nm was found to be highest in winter ( $10.4 \pm 6.76 \text{ Mm}^{-1}$  and  $10.0 \pm 5.13 \text{ Mm}^{-1}$ , respectively) and distinct from season to season. Averages of fluorescence index (FI) and biological index (BIX) of WSBrC were lower in summer than in other seasons and opposite to that of humification index (HIX), which implied that the secondary formation and further chemical processing of aerosols were intensive during the summer period than in other seasons. Whereas in winter, the higher HIX together with the higher FI and BIX of WI-MSBrC suggested that the BrC loading was mainly influenced by primary emissions from biomass burning and coal combustion. Based on EEM, the types of fluorophores in WSBrC were divided into humic-like substances (HULIS), including low-oxygenated and high-oxygenated species, and protein like compounds (PLOM), whereas mostly PLOM in the WI-MSBrC. The direct radiation absorption by both WSBrC and WI-MSBrC in the range of 300–400 nm was accounted for ~40% to that ( $SFE_{Abs}$ ,  $4.97 \pm 2.71 \text{ Wg}^{-1}$  and  $7.58 \pm 5.75 \text{ Wg}^{-1}$ , respectively) in the range, 300–700 nm.

## 1 Introduction

Brown carbon (BrC) is a part of organic aerosol (OA) and can absorb solar radiation in the near-ultraviolet (UV) to visible (Vis) light, ranging from 300–500 nm (Liu et al., 2013). It has been well recognized that BrC has a significant effect on radiative forcing at both regional and global scales (Feng et al., 2013; Jo et al., 2016; Park et al., 2010). *For example*, the warming effect of water-soluble BrC in the Arctic has been reported to be accounted for ~30% of that exerted by the black carbon (Yue et al., 2022). The BrC not only affects the direct radiative forcing, but also has a potential impact on indirect radiative forcing due to its hydrophilicity, which influences the formation of cloud condensation nuclei (CCN) (Andreae and Gelencs'er, 2006; Laskin et al., 2015b). In addition, BrC is mostly composed of highly conjugated aromatic ring compounds such

40 as a polycyclic aromatic hydrocarbons and high molecular weight substances with a polar  
41 functional group that consists of nitrogen and/or oxygen, or humic-like substances (HULIS), which  
42 could pose a risk to human health. *For example*, carbon-containing aromatic compounds can cause  
43 physical weakness, decreased immunity, arteriosclerosis, etc., which will increase the mortality  
44 due to cardiovascular and cerebrovascular diseases and a variety of cancers such as skin cancer,  
45 pharyngeal cancer and nasal cancer (Diggs et al., 2011;Peters et al., 2008;Hecobian et al., 2010).

46 BrC can be emitted directly from primary sources such as biomass burning (Hoffer et al.,  
47 2006;Brown et al., 2021), fossil fuel combustion (Jo et al., 2016), and non-combustion processes  
48 such as bioaerosols (plant debris and fungi) and soil humus (Lin et al., 2014;Rizzo et al.,  
49 2013;Rizzo et al., 2011). On the other hand, BrC can also be produced from complex chemical  
50 reactions of volatile organic compounds (VOCs) emitted from both anthropogenic and biological  
51 origin in gas-phase as well as by multiphase reactions between the gaseous, particulate and  
52 aqueous constituents (Kasthuriarachchi et al., 2020;Li et al., 2020a;Laskin et al., 2015a).

53 In recent times, after establishing the fact that BrC absorb the light, the researchers are paying  
54 lot of attention to measure the physical (optical) and chemical characteristics of the BrC and  
55 estimate its climatic effects (Yue et al., 2019;Choudhary et al., 2021;Hecobian et al., 2010).  
56 However, studies on BrC are still very limited due to difficulties in quantitative measurement of  
57 light-absorbing organic components (Corbin et al., 2019;Wang et al., 2022b). In fact, based on the  
58 disparity in wavelength dependence between BC and BrC, traditional optical instruments can be  
59 used to obtain the BrC absorption value, but the availability of such instruments are limited, which  
60 can accurately and directly differentiate the light absorption caused by the BC and BrC. On the  
61 other hand, the molecular composition and optical properties of BrC are significantly changed  
62 when the BrC is subjected for physical and photo-chemical processing (aging) in the atmosphere.  
63 That is why, the indirect approaches have been developed to explore the molecular composition  
64 including chromophores and sources of BrC through its light absorption and fluorescence  
65 characteristics.

66 UV-Vis spectroscopy and excitation emission matrix (EEM) fluorescence spectroscopy are  
67 considered to be common techniques for studying the optical absorption and fluorescence  
68 chromophore optical and structural characteristics of complex organic materials, because each  
69 chromophore has its own specific excitation-emission peak in the EEM maps (Chen et al.,  
70 2016b;Coble, 2007). In recent years, combined spectrophotometric measurement and chemical  
71 analysis has been applied to study the BrC in Xi'an, Northwest China (Huang et al., 2018). In fact,  
72 EEM fluorescence spectroscopy provides multiple superposed spectral data. By using parallel  
73 factor (PARAFAC) analysis of such spectral data, the type of chromophores can be identified and  
74 their types are quantified semi-quantitatively based on the range of excitation-emission  
75 wavelengths (Cao et al., 2022;Zhan et al., 2022;Murphy et al., 2013). The composition of humic-  
76 like and protein-like components have been identified from the analysis of chromophores of  
77 dissolved organic substances in aquatic environments (Xie et al., 2020). The fluorescence  
78 technique has been widely applied to measure organics in terrestrial and oceanic systems (Murphy  
79 et al., 2013;Yu et al., 2015), but has rarely been used in the study of atmospheric aerosols. Now,  
80 the application of fluorescence technique has been well established in studying the molecular  
81 composition of aerosols as well, the studies on identification of chromophores and thus the  
82 molecular composition of BrC in the atmospheric aerosols are still very limited (Wu et al.,  
83 2021a;Deng et al., 2022;Li et al., 2022;Cao et al., 2022).

84 Therefore, much attention need to be paid further, particularly on long-term and continuous  
85 measurements of the optical characteristics of water-soluble BrC (WSBrC) and their temporal and

86 spatial variations. Moreover, the investigation of light absorption and fluorescence characteristics  
87 of water-insoluble BrC (WIBrC) that can be extracted into a solvent with higher extraction  
88 efficiency is necessary to better understand the impact of the BrC on climate change (Corbin et al.,  
89 2019). In fact, such studies are very scarce, because the selection of solvents and determination of  
90 extraction efficiency are difficult, although different polar chromophores could be extracted by  
91 solvent extraction according to the polarity of solvent and methanol has been used as a common  
92 solvent (Chen et al., 2016a). Hence, the comprehensive study of the optical properties of WSBBrC  
93 and WIBrC is highly necessary to better understand the types of chromophores and optical  
94 properties of atmospheric aerosols, as well as the processes of oxidation and transformations of  
95 chromophores at different locale over the world.

96 China is one of the most polluted areas in the world, and suffering from the absorption and  
97 scattering of solar radiation by atmospheric aerosols that directly affect the energy balance of the  
98 Earth's climate system, especially in North China Plain (Wang et al., 2022a). As an important port  
99 city in the North China Plain, Tianjin, which has a large population, has received a widespread  
100 attention to address the atmospheric environmental issues. Previous studies have shown that BrC  
101 in the atmosphere contributes significantly to the light absorption by aerosols (Deng et al., 2022).  
102 PM<sub>2.5</sub> loading in the Tianjin area is extremely high, with greater abundance of organic matter (OM)  
103 (Dong et al., 2023a). In such an environment, BrC is likely to become an important light-absorbing  
104 component of atmospheric aerosols. However, the studies on physico-chemical characteristics and  
105 sources of BrC are very limited in the North China Plain, and to the best of our knowledge, the  
106 long-term observations of the optical properties and molecular composition of BrC have not been  
107 reported yet over the Tianjin region.

108 In this study, we measured the optical properties and molecular composition of WSBBrC and  
109 water-insoluble but methanol-soluble BrC (WI-MSBrC) in fine aerosols (PM<sub>2.5</sub>) collected from  
110 Tianjin, North China over a one-year period using the combined UV-Vis absorption and EEM  
111 fluorescence spectroscopy technique. We discussed the seasonal variations in optical properties  
112 and chromophore composition of WSBBrC and WI-MSBrC in the PM<sub>2.5</sub>. We also assessed the  
113 possible sources of BrC including the potential photochemical processing of OA (aging) over the  
114 Tianjin region, based on the relationships between the BrC and chemical tracers and stable carbon  
115 ( $\delta^{13}\text{C}$ ) and nitrogen ( $\delta^{15}\text{N}$ ) isotope ratios of total carbon (TC) and nitrogen (TN) in the PM<sub>2.5</sub>. Thus,  
116 this study provides a comprehensive understanding of the optical characteristics, seasonality, and  
117 sources of BrC in the Tianjin region, and warrant the need to develop the prevention and control  
118 strategies for the BrC and/or its precursors emissions.

## 119 **2 Materials and Methods**

### 120 **2.1 Aerosol sampling**

121 Fine aerosol (PM<sub>2.5</sub>) sampling was conducted in Tianjin, a coastal city located at the lower  
122 reaches of the Haihe River and Bohai Sea and 150 km away from Beijing in the northern part of  
123 China. The sampling took place on the rooftop of a six-storey building at Tianjin University (ND,  
124 39.11°N, 117.18°E) in an urban area of Nankai District, Tianjin. A high-volume air sampler (Tisch  
125 Environmental, TE-6070DX) at a flow rate of 1.0 m<sup>3</sup> min<sup>-1</sup> and pre-combusted (6 hours at 450°C)  
126 quartz fiber filters (Pallflex 2500QAT-UP) were used for continuously collecting the PM<sub>2.5</sub>  
127 samples for 3 days (~72 hours) each during 5 July 2018 to 4 July 2019 ( $n = 121$ ). Filter blanks  
128 were collected twice per season during the sample campaign, following the same sampling  
129 procedure placing the filter in hood for 10 mins without turning on the sampler pump.

130 Prior to and after sampling, each filter was dehumidified in a desiccator for 48 hours and  
131 determined the PM<sub>2.5</sub> mass by gravimetric analysis, and then stored in a pre-combusted glass jar  
132 with a Teflon-lined cap in the dark at -20°C until analysis.

## 133 2.2 Measurement of carbonaceous and ionic components

134 Details of the measurements of aerosol organic carbon (OC), element carbon (EC) and water-  
135 soluble organic carbon (WSOC) were described by Wang et al. (Wang et al., 2019) and Dong et  
136 al. (Dong et al., 2023a). Briefly, concentrations of the OC and EC were measured using an aliquot  
137 of filter (1.5. cm<sup>2</sup>) and a thermal-optical carbon analyzer (Sunset Laboratory Inc, USA), following  
138 the IMPROVE protocol of the protective visual environment. WSOC was measured using an  
139 aliquot of filter (one disc of either 14 mm or 22 mm in diameter) extracted into organic-free Milli  
140 Q water and total organic carbon (TOC) analyzer (Model OI, 1030W + 1088). Concentrations of  
141 K<sup>+</sup> and Cl<sup>-</sup> were determined using an aliquot of filter (one disc of 22 mm in diameter) extracted  
142 into ultrapure water (>18.2MΩ cm) and ion chromatography (ICS-5000 System, China, Dai An)  
143 (Dong et al., 2023a). The analytical uncertainty in replicate analyses were within 2 % for OC and  
144 5% for EC, WSOC and inorganic ions. Concentrations of all the components were corrected for  
145 field blanks.

## 146 2.3 Measurement of optical properties of brown carbon (BrC)

### 147 2.3.1 Extraction and concentration of BrC

148 BrC was extracted into 30 ml ultrapure water using a sample filter disc of 22 mm in diameter  
149 placed in a glass bottle with screw cap and sealed with Teflon tape under ultrasonication for 30  
150 min. The extracts were filtered through a 0.45 μm polytetrafluoron (PTFE) syringe filter to remove  
151 the water-insoluble particles and filter debris, and transferred into a clean glass bottle. The extracts  
152 were used for the light absorption and fluorescence measurements of WSBrC. While the  
153 concentration of WSBrC was considered as the concentration of WSOC.

154 After the extraction of WSBrC, the WI-MSBrC was extracted into 30 ml methanol using the  
155 same filter sample left in the same glass bottle with screw cap sealed with Teflon tape under  
156 ultrasonication for 30 min. The extracts were filtered using the same 0.45 μm PTFE syringe filter  
157 to remove the insoluble particles and filter debris and transferred into another clean glass bottle.  
158 The methanol extracts were used for the measurements of optical properties of WI-MSBrC. The  
159 concentration of water-insoluble organic carbon (WIOC) was considered as the concentration of  
160 WI-MSBrC, which calculated as equation (1), presuming that all the water-insoluble organic  
161 contents are dissolved in methanol, although we do not preclude that some of organic species are  
162 not soluble in MeOH (Shetty et al., 2019).

$$163 \quad WI - MSBrC = OC - WSOC \quad (1)$$

### 164 2.3.2 Light absorption of BrC

165 A three-dimensional fluorescence spectrometer (Aqualog, Horiba Scientific) was used to  
166 record the excitation-emission matrices (EEM) spectra and ultraviolet-visible (UV-Vis)  
167 absorption spectra of the solution samples in 1×1 cm quartz cuvettes. The instrument parameters  
168 during sample analysis were as follows: The UV-Vis absorption spectra of extracts were recorded  
169 in the wavelength range of 240–700 nm. The UV-visible absorption spectra of the solvents were  
170 also recorded to subtract their contributions from the extract spectra. The EEM was recorded in  
171 the wavelength range of 240–700 nm for excitation and the integration time was 0.1 s with a 1 nm

172 increment. An increment of 8 pixels (5.04 nm) is used as the emission wavelength interval. Prior  
173 to sample analysis, the pure solvents of water and methanol (MeOH) were used to obtain the  
174 reference signal.

175 Based on the light absorption spectra, the absorption data are converted to the absorption  
176 coefficient ( $Abs: m^{-1}$ ) following equation (2) (Deng et al., 2022; Hecobian et al., 2010):

$$177 \quad Abs_{\lambda} = (A_{\lambda} - A_{700}) \times \frac{V_l}{V_a} \times \ln(10) \quad (2)$$

178 where  $A_{700}$  is the absorption at 700 nm, serving as a reference to account for baseline drift;  $V_l$  is  
179 the volume of water or MeOH used for extraction;  $V_a$  is the volume of sampled air;  $L$  is the optical  
180 path length (0.01 m). A factor of  $\ln(10)$  is utilized to convert the log base 10 to a natural logarithm  
181 to obtain a base-e absorption coefficient. To compensate for any baseline shift that may occur  
182 during analysis, absorption at wavelengths below 700 nm is compared to that of 700 nm where no  
183 absorption occurs for ambient aerosol extracts. The average absorption coefficient between 360  
184 and 370 nm ( $Abs_{365}$ ) is used to represent BrC absorption in order to avoid any interferences from  
185 non-organic compounds (e.g., nitrate) and to be consistent with the literature values (Huang et al.,  
186 2018).

187 Absorption Ångström exponent (AAE, Å) represents the spectral dependence of aerosol light  
188 absorption. The spectral dependence of light absorption by chromophores in solution can be  
189 described by the following equation (3):

$$190 \quad Abs_{\lambda} = C \times \lambda^{-AAE} \quad (3)$$

191 where  $C$  is a composition-dependent constant;  $\lambda$  is the wavelength (nm). The AAE of the filter  
192 extracts is calculated by a formula in the wavelength range of 300–500 nm. The selected range  
193 serves two purposes: (1) to prevent any interferences from non-organic compounds at lower  
194 wavelengths; (2) to ensure a sufficient signal-noise ratio for the investigating samples (Huang  
195 et al., 2018).

196 The mass absorption efficiency (MAE:  $m^2 g^{-1}$ ) of the filter extract at wavelength of  $\lambda$  can be  
197 characterized as equation (4). The ratio of  $MAE_{250}$  to  $MAE_{365}$  is denoted as  $E_2/E_3$  to characterize  
198 the relative size of molecular weight, which is inversely proportional to the molecular weight.  
199  $E_2/E_3$  is calculated with the method as equation (5).

$$200 \quad MAE_{\lambda} = Abs_{\lambda}/M \quad (4)$$

$$201 \quad \frac{E_2}{E_3} = \frac{MAE_{250}}{MAE_{365}} \quad (5)$$

202 where  $M$  ( $\mu g m^{-3}$ ) is the concentration of WSOC for water extracts and that of WIOC for methanol  
203 extracts.

204 The imaginary part ( $k$ ) of the refractive index ( $m = n+ik$ ) is derived with the following  
205 equation (6) (Liu et al., 2013; Deng et al., 2022):

$$206 \quad k_{\lambda} = (MAE \times \rho \times \lambda)/4\pi \quad (6)$$

207 where MAE is the mass-absorption cross section of WSBrC or WI-MSBrC ( $m^2 g^{-1}$ ),  $\rho$  is the  
208 effective density,  $\lambda$  is the wavelength for the computed MAE including WSBrC and WI-MSBrC.  
209 For this study, an effective density of  $1.5 g m^{-3}$  is assumed for WSBrC and WI-MSBrC in the  
210 derivation (Liu et al., 2013). MAE values are computed for 365 nm.

### 211 2.3.2 EEM of BrC and PARAFAC analysis

212 The raw EEMs were first calibrated for the correction of spectrometer factors, which reflect  
213 the spectrometer deviation and light source, and then for the inner filter correction, following the  
214 procedure described elsewhere (Chen et al., 2019; Gu and Kenny, 2009). Briefly, the inner filter

215 correction of the EEMs was done based on the UV-Vis light absorbance of the extracts, which was  
 216 lower than 0.7 in the calibrated wavelength range and is appropriate (Gu and Kenny, 2009). The  
 217 signal intensity of the EEMs was then normalized to the Raman unit (RU) of water (Lawaetz and  
 218 Stedmon, 2009). The fluorescence volume (FV, RU-nm<sup>2</sup>/m<sup>3</sup>) of extracts present in the atmosphere  
 219 was estimated based on the EEMs at the excitation wavelength ranging from 240 to 700 nm, and  
 220 then normalized it (i.e., NFV (RU-nm<sup>2</sup>-[mg/L]<sup>-1</sup>)) by dividing the FV with the concentration of  
 221 WSOC and WIOC in the aerosol [mg m<sup>-3</sup>]).

222 Various types of chromophores present in the PM<sub>2.5</sub> samples were classified and identified  
 223 based on the PARAFAC analysis of the EEMs using the SOLO (Eigenvector Inc.), the data  
 224 analysis software. PARAFAC analysis was performed for each extraction fluid in each season.  
 225 Ultimately, three EEM components were determined and assigned to different types of  
 226 chromophores.

227 Additionally, fluorescence index (FI) was determined by calculating the ratio of emission  
 228 intensities at 450 nm and 500 nm after excitation at 370 nm (McKnight et al., 2001). Contributions  
 229 from local biological sources can be characterized by biological index (BIX), which was calculated  
 230 using the ratio of emission intensities at 380 and 430 nm following 310 nm excitation (Gao yan  
 231 and Zhang, 2018). Under the condition of Ex=255 nm, the humification index (HIX) was  
 232 determined by dividing the area of fluorescence intensity between 435 and 480 nm by that of  
 233 fluorescence intensity between 300 and 345 nm (Battin, 1998). The calculation formulas (7)– 9)  
 234 are as follows:

$$235 \quad FI = \frac{F_{450}}{F_{500}}, \lambda_{Ex} = 370nm \quad (7)$$

$$236 \quad BIX = \frac{F_{380}}{F_{430}}, \lambda_{Ex} = 310nm \quad (8)$$

$$237 \quad HIX = \frac{\int_{435-480}}{\int_{300-345}}, \lambda_{Ex} = 255nm \quad (9)$$

238 In formula (6) - (8),  $\lambda_{Ex}$  refers to the excitation wavelength,  $F_i$  refers to the fluorescence  
 239 intensity of emission wavelength at  $i$  in the emission spectrum, and  $\int_{i-j}$  refers to the integrated  
 240 fluorescence emission intensity in the range of 435–480 nm to 300–345 nm.

### 241 2.3.3 Simple forcing efficiency by light absorption of BrC (SFE<sub>Abs</sub>)

242 It is possible to make a rough estimate of the radiative forcing caused by aerosols using a  
 243 simple forcing efficiency (SFE, W/g), which reflects the energy added to the Earth's atmospheric  
 244 system per unit mass of aerosols and can be estimated as described in the literature (Bond and  
 245 Bergstrom, 2006;Deng et al., 2022), using the following equation (10):

$$246 \quad \frac{dSFE}{d\lambda} = -\frac{1}{4} \frac{dS(\lambda)}{d\lambda} \tau_{atm}^2 (\lambda) (1 - F_c) [2(1 - a_s)^2 \beta(\lambda) \times MSE(\lambda) - 4a_s \times MAE(\lambda)] \quad (10)$$

247 where  $dS/d\lambda$  is the solar irradiance,  $\tau_{atm}$  is the atmospheric transmission (0.79),  $F_c$  is the cloud  
 248 fraction (approximately 0.6),  $a$  is the surface albedo (average 0.19),  $\beta$  is the backscatter fraction,  
 249 and MSE and MAE are the mass scattering and absorption efficiency, respectively (Deng et al.,  
 250 2022).

251 Since BrC causes the radiative effect mainly by light absorption, rather than the scattering  
 252 that has stronger dependency on the particle size, we limited to estimate the radiative effect caused  
 253 by only the absorption of the BrC in this study. Therefore, the equation (10) can be simplified to:

$$254 \quad SFE_{Abs} = \int \frac{dS(\lambda)}{d\lambda} \tau_{atm}^2 (1 - F_c) a_s MAE(\lambda) d\lambda \quad (11)$$

## 255 3 Results and discussion

### 256 3.1 Characteristics of ultraviolet light absorption of WSBrc and WI-MSBrc

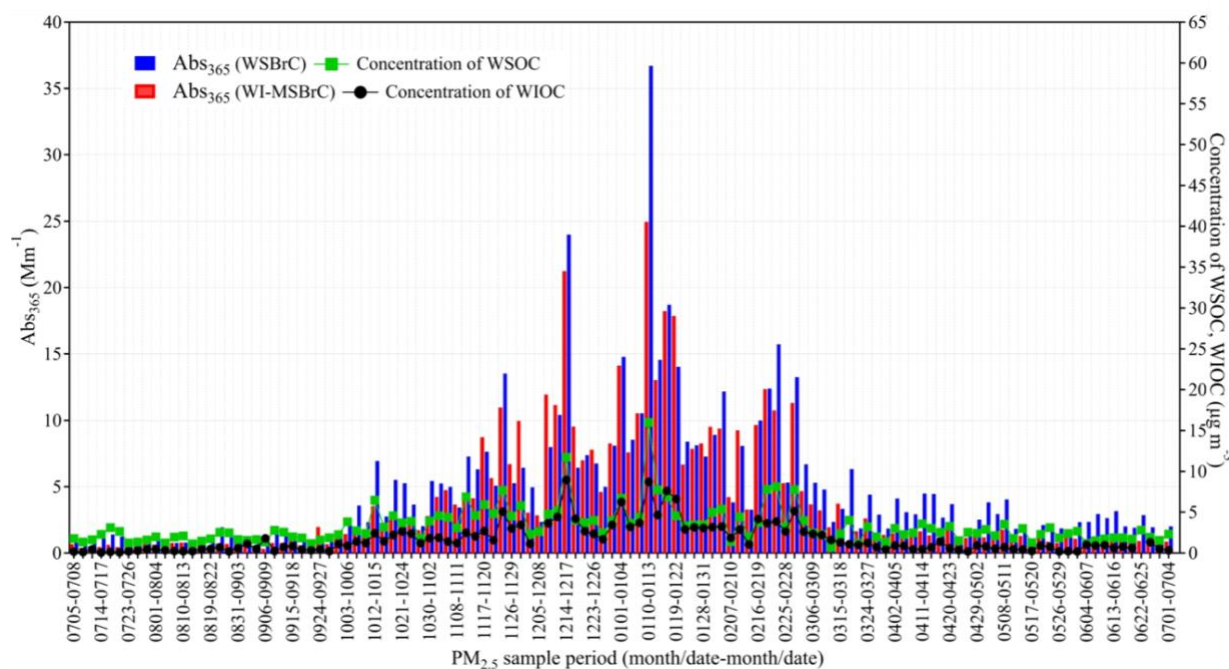
#### 257 3.1.1 Absorption coefficient (Abs)

258 Annual and seasonal averages of various optical properties of WSBrc and WI-MSBrc in  
259 PM<sub>2.5</sub> measured in this study are summarized in Table 1. Their ranges and median values are  
260 provided in supplement Table S1. Temporal variations in absorption coefficient of WSBrc at 365  
261 nm (Abs<sub>365(WSBrc)</sub>) and that of WI-MSBrc (Abs<sub>365(WI-MSBrc)</sub>) together with the concentrations of  
262 WSOC and WIOC are depicted in Fig. 1. Because the light absorption at the wavelength of 365  
263 nm would not be interfered by inorganic substances (Hecobian et al., 2010), the Abs at 365 nm  
264 was selected for the analysis in this study. Abs<sub>365(WSBrc)</sub> ranged from 0.49 Mm<sup>-1</sup> to 36.7 Mm<sup>-1</sup> with  
265 an average of 4.74 Mm<sup>-1</sup> during the campaign. While the Abs<sub>365(WI-MSBrc)</sub> ranged from 0.32-25.0  
266 Mm<sup>-1</sup> (avg. 3.87 Mm<sup>-1</sup>) during the campaign. Temporal trends of Abs<sub>365(WSBrc)</sub> were found to be  
267 similar with those of Abs<sub>365(WI-MSBrc)</sub>, with the lowest levels in summer followed by a gradual  
268 increase toward autumn and peak in winter and then a gradual decrease toward spring during the  
269 campaign (Fig. 1). Furthermore, those trends were highly comparable to those of the  
270 concentrations of both WSOC and WIOC in PM<sub>2.5</sub> (Fig. 1). The correlations between Abs<sub>365(WSBrc)</sub>  
271 and WSOC and Abs<sub>365(WI-MSBrc)</sub> and WIOC were found to be strong (R = 0.93 and 0.96,  
272 respectively) during the campaign. These results indicate that both WSBrc and WI-MSBrc might  
273 have been derived from the same or similar sources including the secondary processes, and their  
274 light absorbance should have been significantly dependent on their abundances that varied from  
275 season to season (Fig. 1; Table 1).

276 Averages of both Abs<sub>365(WSBrc)</sub> and Abs<sub>365(WI-MSBrc)</sub> were higher in winter followed by autumn  
277 and spring and the lowest in summer (Table 1). The high Abs<sub>365</sub> of BrC in winter might have been  
278 mainly driven by the existence of large amounts of organic aerosols, whereas the lowest Abs<sub>365</sub> in  
279 summer might be due to enhanced decomposition of BrC constituents by photobleaching under  
280 high solar radiation and oxidants loading in the atmosphere, which is unlikely in the wintertime.  
281 The seasonal variations of both Abs<sub>365(WSBrc)</sub> and Abs<sub>365(WI-MSBrc)</sub> in Tianjin were similar to those  
282 of the Abs<sub>365</sub> of WSBrc reported in the southeastern United States, but their values (Table 1) were  
283 much higher than that (0.3–3.0 Mm<sup>-1</sup> in 2007) in the southeastern United States (Hecobian et al.,  
284 2010) as well as that in Atlanta and Los Angeles (0.88 ± 0.71 and 0.61 ± 0.38 Mm<sup>-1</sup>, respectively)  
285 in summer 2010 (Zhang et al., 2011). Biomass burning was considered to be the dominant source  
286 of BrC at the southeastern United States in colder period, whereas both primary emissions from  
287 fossil fuel combustion and secondary formation were significant in summertime (Hecobian et al.,  
288 2010). While the SOA formed from fresh anthropogenic and biogenic VOCs were considered to  
289 be major at Atlanta and Los Angeles, respectively (Zhang et al., 2011).

290 It has been reported that the solid fules (i.e., biomass or coal) combustion is dominant and the  
291 Abs<sub>370</sub> of BrC is reported to be high (21.8 Mm<sup>-1</sup>) in North China cities (Zhang et al., 2021). It has  
292 also been reported that the Abs<sub>370</sub> of BrC produced by residential wood burning is much higher,  
293 reaching up to 37.1 ± 74.6 Mm<sup>-1</sup> in Athens in winter (Liakakou et al., 2020). The maximum  
294 Abs<sub>365(WSBrc)</sub> and Abs<sub>365(WI-MSBrc)</sub> in Tianjin aerosols were 36.7 and 25.0 Mm<sup>-1</sup>, respectively,  
295 which are comparable to those of wood combustion samples. However, their ranges found to be  
296 large during the campaign (Fig. 1; Table S1), suggesting that in addition to biomass burning, the  
297 other emission sources and meteorological conditions in different seasons should have been played  
298 an important role in controlling the WSBrc and WI-MSBrc loadings and their optical

299 characteristics in the Tianjin atmosphere. Furthermore, the  $Abs_{365}(WSBrC)$  observed in this study  
 300 (Table 1) is slightly lower compared to that reported in Tianjin during winter 2016 ( $14.1 \pm 8.5$   
 301  $Mm^{-1}$ ) and summer 2017 ( $2.1 \pm 1.0 Mm^{-1}$ ) (Deng et al., 2022) as well as that reported in Beijing  
 302 and Xi'an, which are considered to be highly polluted cities in northern China (Huang et al.,  
 303 2020; Li et al., 2020b). However, the  $Abs_{365}(WSBrC)$  and  $Abs_{365}(WI-MSBrC)$  found in winter in this study  
 304 were higher than that reported at different locations in southern China; Nanjing ( $Abs_{365}(WSBrC) =$   
 305  $4.84 Mm^{-1}$ ,  $Abs_{365}(MSBrC) = 7.75 Mm^{-1}$ ) (Xie et al., 2020), Guangzhou ( $Abs_{365}(WSBrC) = 8.8 Mm^{-1}$ )  
 306 (Li et al., 2018), and Lhasa ( $Abs_{365}(WSBrC) = 1.04 Mm^{-1}$ ,  $Abs_{365}(MSBrC) = 1.47 Mm^{-1}$ ) (Zhu et al.,  
 307 2018), where the fossil fuel combustion is considered as the dominant source. Such higher  $Abs_{365}$ ,  
 308 particularly in winter, indicates that BrC in  $PM_{2.5}$  in Tianjin might have been derived from mixed  
 309 sources such as biomass burning and fossil fuel (coal) combustion and has a significant effect on  
 310 light absorption and thus on climate system over the region.



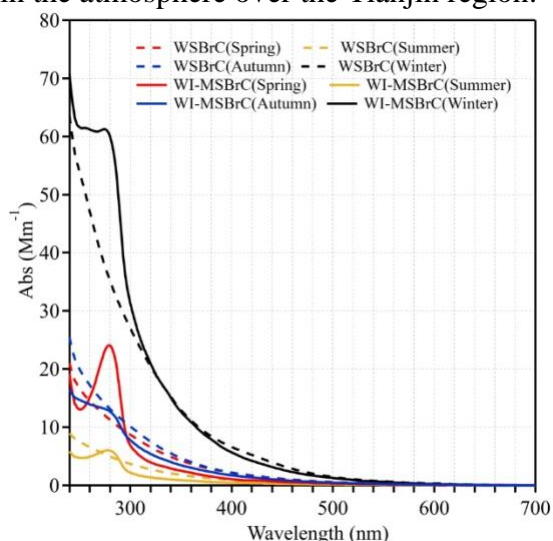
311  
 312 **Figure 1.** Temporal variations of the light absorption coefficient of water-soluble brown carbon  
 313 (BrC) at 365 nm ( $Abs_{365}(WSBrC)$ ) and water-insoluble but methanol-soluble BrC ( $Abs_{365}(WI-MSBrC)$ )  
 314 and the mass concentrations of WSOC and WIOC in  $PM_{2.5}$  in Tianjin, North China during 2018  
 315 and 2019. WSOC and WIOC mass concentrations data was obtained from (Dong et al., 2023b).

316 Figure 2 shows the seasonal average absorption spectra of WSBrC and WI-MSBrC at  
 317 wavelengths of 240–700 nm, which shows a common feature that the absorption of shorter  
 318 wavelengths increases sharply and significantly. Such feature is different from the absorption  
 319 characteristics of BC, whose AAE is close to 1 and weakly dependent on the wavelength. Another  
 320 evident feature of BrC absorption spectra shown in Figure 2 is that the Abs of WI-MSBrC was  
 321 always greater than that of WSBrC across the shorter wavelengths in winter and in the range of  
 322 260~300 nm in other seasons, which is consistent with the pattern reported in the literature (Huang  
 323 et al., 2020; Li et al., 2020b). In addition, the Abs of WI-MSBrC peaked at 280 nm, but not that of  
 324 WSBrC (Fig. 2). Such patterns can be attributed to the difference in types and amounts of  
 325 chromophores soluble in water and methanol (e.g., PAHs are soluble in methanol, but not in water).



326 It is noteworthy that,  $\pi-\pi^*$  electron transitions in the double bonds of aromatic compounds are the  
327 primary cause of light absorption in the wavelength range of 250–300 nm. It has been reported in  
328 another study that nitroaromatics have contributed 60% to the total absorbance in the 300-400 nm  
329 range (Hems et al., 2021). The electron transitions in phenolic arenes, aniline derivatives, polyenes  
330 and polycyclic aromatic hydrocarbons with two or more rings are responsible for the absorbance  
331 in the bands between 270 and 280 nm (Baduel et al., 2009). Therefore, the differences observed in  
332 the Abs of WSBrc and WI-MSBrc imply that the aromatic and/or unsaturated aliphatic organic  
333 compounds are abundant in PM<sub>2.5</sub> in Tianjin, which are more soluble in MeOH than in water.

334 High correlations ( $R = 0.73-0.97$ ) were found between Abs<sub>365</sub> of both WSBrc and WI-  
335 MSBrc and WSOC and WIOC in each season, except in summer ( $R = 0.20-0.62$ ) (Figure S1). As  
336 noted earlier, such linearity of Abs<sub>365</sub> with WSOC and WIOC indicate that WSBrc and WI-  
337 MSBrc might have been derived from similar sources including the secondary processes over the  
338 Tianjin region, except in summer, because the light absorption efficiency of organic compounds  
339 of different origin are different and significantly depend on their secondary processes in the  
340 atmosphere (Zhong and Jang, 2011). In fact, the Abs depends on the amount of BrC availability,  
341 but not of total OC content. In summer, the BrC loading might be less due to either photobleaching  
342 under the enhanced aging and/or less availability of N and/or S species to produce N- and S-  
343 containing organics (BrC) in the atmosphere over the Tianjin region.



344  
345 **Figure 2.** Seasonal averages of absorption spectra in the wavelength range of 240–700 nm of  
346 WSBrc and WI-MSBrc in PM<sub>2.5</sub> from Tianjin, North China.

347 The moderate to high positive correlations ( $R = 0.51-0.92$ ) found between both Abs<sub>365</sub>(WSBrc)  
348 and Abs<sub>365</sub>(WI-MSBrc) and  $K^+$  and  $Cl^-$  in all seasons, except between Abs<sub>365</sub> WSBrc and  $Cl^-$  in summer  
349 ( $R = 0.29$ ) (Fig. S2), suggest that biomass burning and coal combustion were major sources (Dong  
350 et al., 2023a) of BrC in the Tianjin region. The poor correlation between Abs<sub>365</sub> and  $K^+$  was driven  
351 by two outliers obtained in  $K^+$  data that might have occurred due to unknown biomass burning  
352 events at local scale. In addition, the correlation between Abs<sub>365</sub>(WSBrc) and  $K^+$  was relatively  
353 stronger than that between the Abs<sub>365</sub>(WI-MSBrc) and  $K^+$ , except in summer (Fig. S2), which support  
354 that the chromophores, like nitrophenols, derived from biomass burning are potentially more  
355 water-soluble (Li et al., 2020b). While the correlation between Abs<sub>365</sub>(WI-MSBrc) and  $Cl^-$  was  
356 relatively stronger than that between Abs<sub>365</sub>(WSBrc) and  $Cl^-$  in spring and summer and comparable

357 in autumn, which suggest that the chromophores derived from fossil fuel (e.g., coal) combustion  
358 are slightly more soluble in MeOH compared to that in water, and were abundant in the spring and  
359 summer time in Tianjin.  
360

**Table 1.** Mass concentrations of WSOC, WIOC and absorbance efficiency of WSBrC and WI-MSBrC (Avg.  $\pm$  SD) in PM<sub>2.5</sub> from Tianjin, North China.

	Annual	Summer	Autumn	Winter	Spring
<b>Concentrations</b>					
WSOC ( $\mu\text{g m}^{-3}$ )	3.25 $\pm$ 2.18	1.88 $\pm$ 0.53	3.45 $\pm$ 1.71	5.06 $\pm$ 2.99	2.48 $\pm$ 0.82
WIOC ( $\mu\text{g m}^{-3}$ )	1.68 $\pm$ 1.77	0.43 $\pm$ 0.32	1.55 $\pm$ 1.04	3.74 $\pm$ 2.09	0.88 $\pm$ 0.63
<b>Optical parameters</b>					
Abs <sub>365</sub> (Mm <sup>-1</sup> )	4.74 $\pm$ 5.10	1.47 $\pm$ 0.77	3.71 $\pm$ 2.83	10.4 $\pm$ 6.76	3.45 $\pm$ 2.29
MAE <sub>365</sub> (m <sup>2</sup> g <sup>-1</sup> )	1.28 $\pm$ 0.66	0.80 $\pm$ 0.44	0.96 $\pm$ 0.33	2.04 $\pm$ 0.46	1.31 $\pm$ 0.55
AAE (300–500 nm)	5.66 $\pm$ 0.82	5.17 $\pm$ 0.83	6.21 $\pm$ 0.65	5.88 $\pm$ 0.58	5.42 $\pm$ 0.74
E <sub>2</sub> /E <sub>3</sub>	5.36 $\pm$ 0.91	5.64 $\pm$ 1.21	5.78 $\pm$ 0.83	5.19 $\pm$ 0.44	4.83 $\pm$ 0.64
FI	1.38 $\pm$ 0.09	1.31 $\pm$ 0.07	1.47 $\pm$ 0.07	1.37 $\pm$ 0.02	1.37 $\pm$ 0.09
BIX	1.05 $\pm$ 0.13	0.91 $\pm$ 0.06	1.06 $\pm$ 0.08	1.20 $\pm$ 0.08	1.01 $\pm$ 0.11
HIX	2.87 $\pm$ 0.53	3.12 $\pm$ 0.44	3.11 $\pm$ 0.51	2.47 $\pm$ 0.43	2.76 $\pm$ 0.47
k <sub>365</sub>	0.056 $\pm$ 0.029	0.035 $\pm$ 0.020	0.042 $\pm$ 0.015	0.089 $\pm$ 0.021	0.057 $\pm$ 0.024
SFE <sub>Abs300–400</sub> (W g <sup>-1</sup> )	1.95 $\pm$ 1.02	1.21 $\pm$ 0.67	1.99 $\pm$ 0.84	3.12 $\pm$ 0.71	1.46 $\pm$ 0.52
SFE <sub>Abs300–700</sub> (W g <sup>-1</sup> )	4.97 $\pm$ 2.71	3.68 $\pm$ 2.58	5.12 $\pm$ 2.17	7.60 $\pm$ 2.17	3.39 $\pm$ 1.42
<b>WSBrC</b>					
Abs <sub>365</sub> (Mm <sup>-1</sup> )	3.87 $\pm$ 4.69	0.74 $\pm$ 0.25	2.83 $\pm$ 2.51	10.0 $\pm$ 5.13	1.99 $\pm$ 1.95
MAE <sub>365</sub> (m <sup>2</sup> g <sup>-1</sup> )	2.36 $\pm$ 1.26	2.50 $\pm$ 1.78	1.86 $\pm$ 1.02	2.69 $\pm$ 0.36	2.41 $\pm$ 1.28
AAE (300–500 nm)	6.06 $\pm$ 1.23	5.49 $\pm$ 1.26	6.11 $\pm$ 1.86	6.30 $\pm$ 0.27	6.27 $\pm$ 0.90
E <sub>2</sub> /E <sub>3</sub>	6.60 $\pm$ 2.04	6.79 $\pm$ 1.32	5.77 $\pm$ 1.35	6.20 $\pm$ 0.44	7.60 $\pm$ 3.25
FI	1.60 $\pm$ 0.13	1.58 $\pm$ 0.12	1.57 $\pm$ 0.06	1.73 $\pm$ 0.11	1.51 $\pm$ 0.11
BIX	1.26 $\pm$ 0.21	1.32 $\pm$ 0.18	1.05 $\pm$ 0.14	1.43 $\pm$ 0.09	1.23 $\pm$ 0.18
HIX	0.81 $\pm$ 0.60	0.25 $\pm$ 0.08	1.23 $\pm$ 0.61	1.33 $\pm$ 0.30	0.42 $\pm$ 0.28
k <sub>365</sub>	0.104 $\pm$ 0.057	0.109 $\pm$ 0.079	0.081 $\pm$ 0.045	0.117 $\pm$ 0.016	0.105 $\pm$ 0.057
SFE <sub>Abs300–400</sub> (W g <sup>-1</sup> )	2.98 $\pm$ 1.70	1.21 $\pm$ 0.67	2.98 $\pm$ 1.52	4.13 $\pm$ 0.57	3.61 $\pm$ 1.91
SFE <sub>Abs300–700</sub> (W g <sup>-1</sup> )	7.58 $\pm$ 5.75	3.68 $\pm$ 2.58	8.69 $\pm$ 9.23	9.36 $\pm$ 4.51	8.70 $\pm$ 5.03
<b>WI-MSBrC</b>					

## 3.1.2 Absorption Ångström exponent (AAE)

364 The magnitude of the AAE can reflect the sources and atmospheric chemical processes of  
365 BrC (Lack et al., 2013), because the AAE of the BrC emitted from fossil fuel combustion found  
366 to be  $\sim 1$  and that from biomass burning range from 1 to 3 and that derived by secondary  
367 formation/transformations vary from 3-7 (Yan et al., 2018). It has also been reported that the AAE  
368 of light-absorbing organic species (i.e., BrC) is much larger than that of soot (BC). The AAE was  
369 found to be between 2 and 4 for the particles containing both soot and BrC. Furthermore, AAE  
370 value of particulate matter is closely related to its chemical composition, mixing state, particle size  
371 and other factors. *For example*, Sun et al. (2007) reported that the average AAE of coal briquettes  
372 is  $2.55 \pm 0.44$  whereas that of the coal chunks is  $1.30 \pm 0.32$  (Sun et al., 2017). However, it is  
373 important to note that unlike the direct measurement of AAE of the particulate matter, the light  
374 absorption characteristics of organic components extracted into solvent are not affected by particle  
375 size and mixing state of aerosols, but depend on their composition. The AAE of humic-like  
376 substances (HULIS) isolated from biomass burning aerosols by water extraction followed by the  
377 separation with exchange column was reported to be 6-7 (Hoffer et al., 2006).

378 The AAE of WSBrC in PM<sub>2.5</sub> from Tianjin ranged from 3.85 to 7.99 with an average of 5.66  
379 during the campaign. The seasonal averages were highly comparable with each other, except a  
380 little higher level in autumn (Table 1). The average AAE of WSBrC in Tianjin (Table 1) is  
381 comparable to that ( $5.1 \pm 2.0$ ) reported from New Delhi, India and Beijing ( $5.3 \pm 0.4$  in winter and  
382  $5.8 \pm 0.5$  in summer) and the outflow region ( $6.4 \pm 0.6$ ) of northern China (Lesworth et al., 2010).  
383 The AAE of WSBrC in Tianjin was also similar to that (range, 6–8) reported in the particulate  
384 matter at the southeastern United States (Hecobian et al., 2010) and downtown Atlanta (Liu et al.,  
385 2013), where both biogenic and fossil fuel combustion emissions and secondary processes are  
386 considered as significant sources. Such higher levels and comparisons of the AAE of WSBrC  
387 imply that the OA in Tianjin should have been derived from mixed sources and substantially polar,  
388 because the AAE of BrC is increased with its increasing polarity (Chen et al., 2016a).

389 However, the AAE of WI-MSBrC in Tianjin ranged from 2.08–12.9 (avg. 6.06) and was  
390 comparable with that of WSBrC. Furthermore, the averages of AAE of WI-MSBrC in each season  
391 were comparable with the other, except a relatively lower level in summer, and also with those of  
392 the AAE of WSBrC (Table 1). Generally, the water insoluble portion is expected to have a stronger  
393 absorption and weaker wavelength dependence (Saleh, 2020). It has also been reported that the  
394 AAE values of the water extract are greater than those of the acetone and methanol extracts (Shetty  
395 et al., 2019), and interpreted that the extraction efficiency of polycyclic aromatic hydrocarbons  
396 from methanol or other organic solvents is higher than that from water, leading to a higher  
397 absorption at longer wavelengths in the methanol extract and therefore a lower AAE value.  
398 However, it has also been found that the value of AAE<sub>300-600</sub> of water extract of biomass burning  
399 samples is lower than that extracted into acetonitrile (Lin et al., 2017), indicating that the origin of  
400 the BrC is also play an important role. Such comparability between the AAE of WSBrC and WI-  
401 MSBrC is consistent with the pattern reported in urban Beijing during winter and Xi'an, China (Li  
402 et al., 2020b), where the emissions from fossil fuel combustion are dominant. These results and  
403 their comparisons again support that the BrC might have significantly derived from mixed sources  
404 (biomass burning and fossil fuel combustion).

406 MAE provides the light absorbing ability of BrC. The MAE<sub>365</sub> of WSB<sub>r</sub>C (MAE<sub>365(WSB<sub>r</sub>C)</sub>)  
407 ranged from 0.38 m<sup>2</sup> g<sup>-1</sup> to 3.41 (avg. 1.28 m<sup>2</sup> g<sup>-1</sup>) and lower by 2 times than that (range, 0.18-7.05  
408 m<sup>2</sup> g<sup>-1</sup>; avg. 2.36 m<sup>2</sup> g<sup>-1</sup>) of WI-MSB<sub>r</sub>C (MAE<sub>365(WI-MSB<sub>r</sub>C)</sub>) during the campaign in Tianjin.  
409 Although the seasonal averages of both MAE<sub>365(WSB<sub>r</sub>C)</sub> and MAE<sub>365(WI-MSB<sub>r</sub>C)</sub> were higher in winter  
410 (1.28 and 2.36 m<sup>2</sup>g<sup>-1</sup>, respectively), the former showed the second most value in spring followed  
411 by autumn and the lowest value in summer, whereas the latter showed second most value in  
412 summer followed by spring and the lowest value in autumn (Table 1). Furthermore, the average  
413 MAE<sub>365(WSB<sub>r</sub>C)</sub> in winter was 2.5 times higher than that in summer, which is similar to that (1.8  
414 times) reported earlier in Tianjin (Deng et al., 2022), whereas the difference between the averages  
415 of MAE<sub>365(WI-MSB<sub>r</sub>C)</sub> in winter to autumn is 1.4 times only. The seasonal variations of MAE<sub>365(WSB<sub>r</sub>C)</sub>  
416 and MAE<sub>365(WI-MSB<sub>r</sub>C)</sub> found in this study are similar to those reported in Xi'an (Li et al., 2020b).

417 The imaginary refractive index ( $k$ ) is another important parameter that represent the light  
418 absorbing ability of carbon and applied in climate model to assess the direct radiative forcing of  
419 aerosols. The  $k$  of WSB<sub>r</sub>C ( $k_{365(WSB<sub>r</sub>C)}$ ) and WI-MSB<sub>r</sub>C ( $k_{365(WI-MSB<sub>r</sub>C)}$ ) in Tianjin ranged from  
420 0.017 to 0.149 and 0.008-0.307, respectively, in Tianjin. Interestingly, the average  $k_{365(WI-MSB<sub>r</sub>C)}$   
421 was 1.9 times to that of  $k_{365(WSB<sub>r</sub>C)}$  during the campaign (Table 1) and their seasonal patterns were  
422 also exactly similar to those of the MAE<sub>365(WSB<sub>r</sub>C)</sub> and MAE<sub>365(WI-MSB<sub>r</sub>C)</sub> (Table 1).

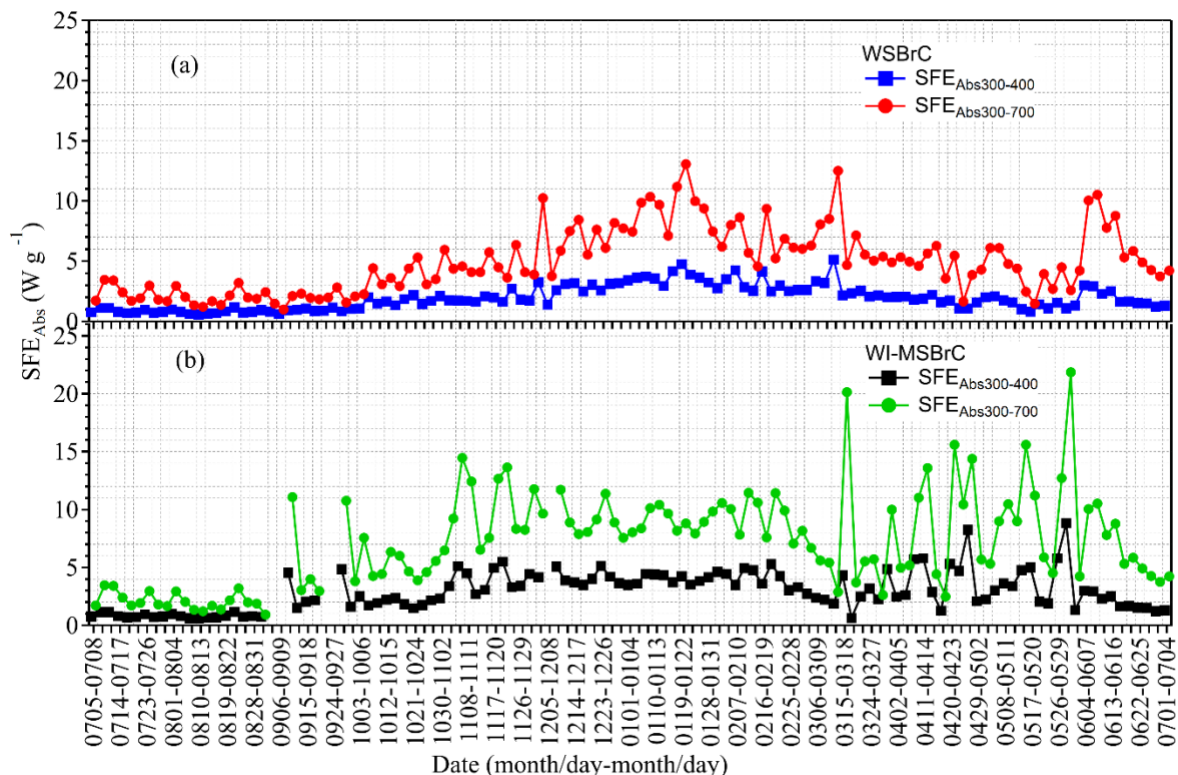
423 Both these MAE<sub>365</sub> and  $k_{365}$  results indicate that most of light-absorbing chromophores are  
424 insoluble in water but soluble in MeOH, and their abundances are significantly varied from season  
425 to season. Such large seasonal differences indicate that the BrC sources and formation and/or  
426 transformation including the degradation (photobleaching) processes might be different in each  
427 season. The higher levels of MAE<sub>365</sub> and  $k_{365}$  in winter suggest that the contributions of OA from  
428 coal combustion and biomass burning emissions were significantly higher than that in other  
429 seasons due to increased residential heating activities. The lower MAE<sub>365(WSB<sub>r</sub>C)</sub> and  $k_{365(WSB<sub>r</sub>C)}$  and  
430 the second most values of MAE<sub>365(WI-MSB<sub>r</sub>C)</sub> and  $k_{365(WI-MSB<sub>r</sub>C)}$  in summer imply that the  
431 contributions of OA from fossil fuel combustion emissions might be dominant and the subsequent  
432 photobleaching of WSB<sub>r</sub>C might be significant under high solar radiation in the summertime.

433 The ratio of MAE<sub>250</sub> to MAE<sub>365</sub>, which is inversely correlate with the molecular size and  
434 aromaticity (Chen et al., 2016c), of WSB<sub>r</sub>C ( $E_2/E_{3(WSB<sub>r</sub>C)}$ ) and WI-MSB<sub>r</sub>C ( $E_2/E_{3(WI-MSB<sub>r</sub>C)}$ ) in  
435 Tianjin ranged from 3.30 to 6.25 with an average of 4.83 and 4.50-24.1 (avg. 7.61), respectively,  
436 during the campaign. Interestingly, the averages of  $E_2/E_{3(WSB<sub>r</sub>C)}$  were comparable in summer and  
437 autumn and higher than that in winter and spring (Table 1). Whereas the average  $E_2/E_{3(WI-MSB<sub>r</sub>C)}$   
438 was higher in spring followed by summer and winter and the lowest in autumn, and higher than  
439 the  $E_2/E_{3(WSB<sub>r</sub>C)}$  in each season, except in autumn. Both  $E_2/E_{3(WSB<sub>r</sub>C)}$  and  $E_2/E_{3(WI-MSB<sub>r</sub>C)}$  in each  
440 season were comparable or relatively higher than the  $E_2/E_3$  of HULIS ( $4.7 \pm 0.27$  for herbaceous  
441 plants,  $3.6 \pm 0.18$  for shrubs,  $4.2 \pm 0.77$  for evergreen trees,  $4.0 \pm 0.82$  for deciduous trees,  $5.8 \pm$   
442  $0.5$  for rice straw,  $4.5 \pm 0.2$  for corn straw and  $4.4 \pm 0.3$  for pine branches) emitted from biomass  
443 burning (Tang et al., 2020) and lower than that ( $14.7 \pm 0.7$ ) of HULIS emitted from coal  
444 combustion (Fan et al., 2016). Thus, the  $E_2/E_{3(WSB<sub>r</sub>C)}$  and  $E_2/E_{3(WI-MSB<sub>r</sub>C)}$  and their comparisons  
445 with source signatures indicate that both WSB<sub>r</sub>C and WI-MSB<sub>r</sub>C in PM<sub>2.5</sub> over the Tianjin region  
446 should have been mainly derived from biomass burning followed by coal combustion and consist  
447 of high aromaticity and large in molecular size.

449 Radiative forcing efficiency of WSBrc and WI-MSBrc were calculated by integrating the  
 450 wavelength dependent  $SFE_{Abs}$  from 300 nm to 700 nm ( $SFE_{Abs300-700}(WSBrc)$  and  $SFE_{Abs300-700}(WI-$   
 451  $MSBrc)$ , respectively) in this study. The  $SFE_{Abs300-400}$  was also integrated to estimate the radiative  
 452 forcing efficiency of WSBrc ( $SFE_{Abs300-400}(WSBrc)$ ) and WI-MSBrc ( $SFE_{Abs300-400}(WI-MSBrc)$ ),  
 453 because the BrC strongly absorbs light in the UV-Vis range. The temporal variations of  $SFE_{Abs}$  of  
 454 WSBrc and WI-MSBrc in both the wavelength ranges are shown in Fig. 3.  $SFE_{Abs300-700}(WSBrc)$   
 455 and  $SFE_{Abs300-400}(WSBrc)$  ranged from  $0.98 \text{ Wg}^{-1}$  to  $13.1 \text{ Wg}^{-1}$  with an average of  $4.97 \text{ Wg}^{-1}$  and  
 456  $0.60\text{-}5.13 \text{ Wg}^{-1}$  (avg.  $1.95 \text{ Wg}^{-1}$ ), respectively. Whereas the  $SFE_{Abs300-700}(WI-MSBrc)$  and  $SFE_{Abs300-}$   
 457  $400(WI-MSBrc)$  were  $0.92\text{-}51.3 \text{ Wg}^{-1}$  ( $7.58 \text{ Wg}^{-1}$ ) and  $0.64\text{-}8.84 \text{ Wg}^{-1}$  ( $2.98 \text{ Wg}^{-1}$ ), respectively, and  
 458 were higher by 1.5 times than that of the  $SFE_{Abs300-700}(WSBrc)$  and  $SFE_{Abs300-400}(WSBrc)$  (Table 1).  
 459 Further both integrated average  $SFE_{Abs300-700}(WSBrc)$  and  $SFE_{Abs300-700}(WI-MSBrc)$  were higher by 2.5  
 460 times to that of the  $SFE_{Abs300-400}(WSBrc)$  and  $SFE_{Abs300-400}(WI-MSBrc)$  (Table 1). Temporal variations  
 461 of both the  $SFE_{Abs300-400}(WSBrc)$  and  $SFE_{Abs300-700}(WSBrc)$  were found to be quite similar with a clear  
 462 seasonal pattern with the lowest levels in summer followed by a gradual increase toward autumn  
 463 to peak in winter and then a gradual decrease toward spring to the lowest levels in summer, except  
 464 a sharp rise in early summer 2019 (Fig. 3). Whereas the  $SFE_{Abs300-400}(WI-MSBrc)$  and  $SFE_{Abs300-700}(WI-$   
 465  $MSBrc)$  showed exactly the similar temporal pattern with each other, but different from that of the  
 466  $SFE_{Abs300-400}(WSBrc)$  and  $SFE_{Abs300-700}(WSBrc)$  (Fig.3). The levels of  $SFE_{Abs300-400}(WI-MSBrc)$  and  
 467  $SFE_{Abs300-700}(WI-MSBrc)$  found to be relatively stable throughout each season, except in spring, with  
 468 higher level in spring followed by winter and lower levels in summer (Fig. 3). In consistent with  
 469 these seasonal patterns, the seasonal variations of  $k_{365}(WSBrc)$  and  $k_{365}(WI-MSBrc)$ , a vital parameter  
 470 that reflect the light absorbing ability and used in the estimation of radiative forcing by climatic  
 471 model (Shamjad et al., 2016), were also showed the similar pattern (Fig. S3).

472 The  $SFE_{Abs}$  of both WSBrc and WI-MSBrc in both the spectral ranges were higher in winter  
 473 (Table 1). However,  $SFE_{Abs300-400}(WSBrc)$  and  $SFE_{Abs300-700}(WSBrc)$  showed the second higher values  
 474 in autumn and the lowest and comparable values in summer and spring (Table 1). Whereas  
 475  $SFE_{Abs300-400}(WI-MSBrc)$  and  $SFE_{Abs300-700}(WI-MSBrc)$  showed the second higher and comparable values  
 476 in spring and autumn and the lowest values in summer (Table 1). It is noteworthy that the  
 477  $SFE_{Abs300-400}(WSBrc)$ ,  $SFE_{Abs300-700}(WSBrc)$ ,  $SFE_{Abs300-400}(WI-MSBrc)$  and  $SFE_{Abs300-700}(WSBrc)$  were  
 478 higher by 61%, 52%, 71% and 61%, respectively, in winter than those in summer, indicating that  
 479 BrC abundance and strong light absorption capacity of BrC in winter led to a significant increase  
 480 in direct radiative forcing by the BrC. Furthermore,  $SFE_{Abs300-400}$  accounted for 40% of  $SFE_{Abs300-}$   
 481  $700$  in both the fractions of BrC during the whole campaign period and their seasonal averages  
 482 varied between 33-44%, which are similar to that reported in Tianjin by Deng et al. (2022),  
 483 indicating the light absorption by BrC in UV-Vis range play a significant role in the total BrC  
 484 radiative forcing.

485 Furthermore, it is important to note that it has been reported that direct radiative effect of  
 486 WSBrc is 12.5% and 13.5% relative to black carbon (BC) radiative forcing in the 280-4000 nm  
 487 range in summer and winter, respectively, in Tianjin (Deng et al., 2022). In fact, as noted above,  
 488 the annual average  $SFE_{Abs300-700}(WI-MSBrc)$  is higher by 1.5 times to that of  $SFE_{Abs300-700}(WSBrc)$   
 489 (Table 1) in Tianjin. Therefore, the direct radiative effect of total ( $\sum WSBrc+WI-MSBrc$ ) BrC  
 490 relative to BC would become  $\sim 32.5\%$  in Tianjin, revealing that the BrC play a greater role in light  
 491 absorbing aerosols in the shorter wavelength region in comparison to the entire spectrum.



492

493 **Figure 3.** Temporal variations in  $SFE_{Abs}$  of WSBrc and WI-MSBrc from 300–400nm and 300–  
 494 700nm in  $PM_{2.5}$  from Tianjin.

495 3.3 Fluorescence characteristics of WSBrc and WI-MSBrc

496 3.3.1 Fluorescence indices

497 Annual and seasonal averages of the fluorescence indices: FI, BIX and HIX, of WSBrc  
 498 ( $FI_{WSBrc}$ ,  $BIX_{WSBrc}$  and  $HIX_{WSBrc}$ , respectively) and WI-MSBrc ( $FI_{WI-MSBrc}$ ,  $BIX_{WI-MSBrc}$  and  
 499  $HIX_{WI-MSBrc}$ , respectively) in  $PM_{2.5}$  at Tianjin are presented in Table 1. Their ranges and median  
 500 values are provided in Table S1, and temporal variations are depicted in Fig. 3. Fluorescence  
 501 indices are developed as indicators for the type and source of the fluorescent organic matter (OM)  
 502 in aquatic and soil systems and has been successfully applied to assess the sources and aging  
 503 processes of OA in the atmosphere in recent times (Dong et al., 2023b; Lee et al., 2013; Wu et al.,  
 504 2021b). FI and BIX provide the insights in exploring the source and aging of OA and received  
 505 much attention in recent times (Xie et al., 2020; Gao yan and Zhang, 2018; Qin et al., 2018; Deng  
 506 et al., 2022). They have been considered as indicators to assess the relative contributions of  
 507 terrestrial, biological and microbially derived OM to OA. The FI values of OM lower than 1.4  
 508 indicate its terrestrial origin and the values of 1.9 or higher indicate the microbial origin, and shows  
 509 an inverse relationship with aromaticity of the OM (Gao yan and Zhang, 2018; Birdwell and Engel,  
 510 2010). The BIX values of 0.8 and 1.0 correspond to the freshly derived OM of biological or  
 511 microbial origin and those of  $\sim 0.6$  imply the little contribution of the biological OM (Birdwell and  
 512 Engel, 2010; Dong et al., 2023b). HIX reflect the degree of humification of OA, and has been  
 513 considered as a proxy for aromaticity of OM and the HIX value is increased with the increasing

514 aromaticity and polycondensation degree (Deng et al., 2022;McKnight et al., 2001;Birdwell and  
515 Engel, 2010). The HIX values of >5 reflect the fresh OM derived from biomass and animal manure  
516 (Birdwell and Engel, 2010).

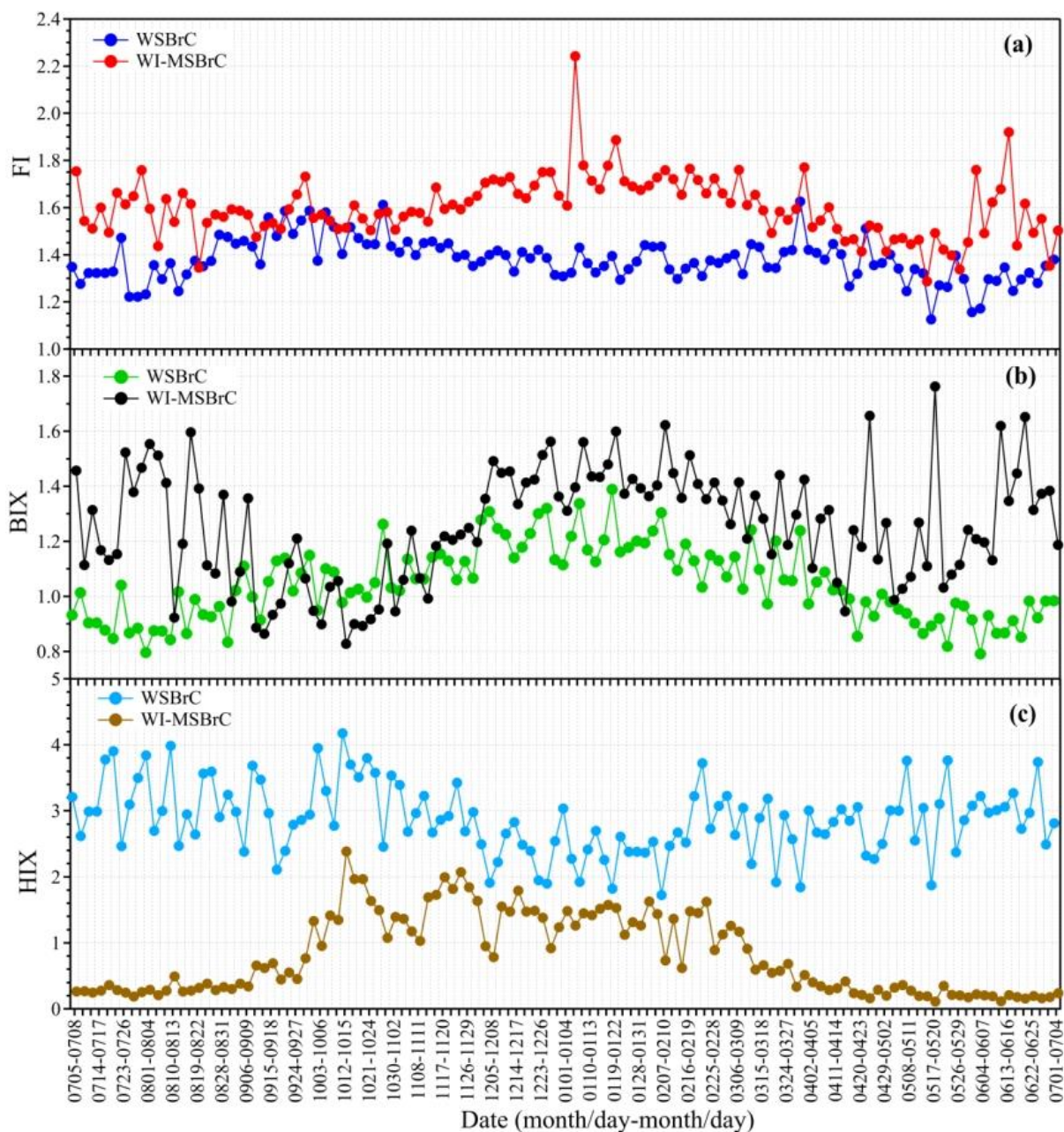
517  $FI_{WSBrC}$  and  $FI_{WI-MSBrC}$  were ranged from 1.13 to 1.63 with an average of 1.38 and 1.29-2.24  
518 (avg. 1.60), respectively, during the campaign in Tianjin. While  $BIX_{WSBrC}$  and  $BIX_{WI-MSBrC}$  were  
519 0.79-1.39 (1.05) and 0.83-1.76 (1.26), respectively, during the campaign. Both FI and BIX of  
520  $WSBrC$  and  $WI-MSBrC$  followed a temporal pattern, but the temporal pattern of  $FI_{WSBrC}$  was  
521 exactly opposite to that of the  $FI_{WI-MSBrC}$  (Fig. 4a). The  $FI_{WSBrC}$  values were slightly decreased  
522 from summer to autumn followed by a gradual increase to mid-winter and then a gradual decrease  
523 to summer through spring (Fig. 4a). While the temporal variations of  $BIX_{WSBrC}$  showed a gradual  
524 decrease from summer to autumn followed by a gradual increase to winter and remained relatively  
525 stable during the wintertime followed by a gradual decrease to to summer through spring (Fig. 4b).  
526 The temporal variations of  $BIX_{WI-MSBrC}$  were also found to be opposite to those of the  $BIX_{WSBrC}$ ,  
527 except in winter, in which the  $BIX_{WI-MSBrC}$  values were higher compared to those in other seasons  
528 (Fig. 4b). Interestingly, the temporal patterns of  $HIX_{WSBrC}$  and  $HIX_{WI-MSBrC}$  were found to be  
529 similar with relatively stable in summer followed by a sharp increase in early autumn and then a  
530 gradual decrease to summer through winter and spring (Fig. 4c). Further the  $HIX_{WSBrC}$  was always  
531 significantly higher than the  $HIX_{WI-MSBrC}$ . Such temporal differences in all the three fluorescence  
532 indices clearly indicate that the composition and/or aromaticity of  $WSBrC$  and  $WI-MSBrC$  are  
533 substantially distinct, even though they might have been mainly derived from similar sources:  
534 biomass burning and coal combustion, as discussed in previous section.

535 Average  $FI_{WSBrC}$  was found to be higher in autumn followed the similar levels in winter and  
536 spring and the lowest in summer, whereas that of  $BIX_{WSBrC}$  was higher in winter followed by  
537 autumn, spring and the lowest in summer (Table 1). While the averages of both  $FI_{WI-MSBrC}$  and  
538  $BIX_{WI-MSBrC}$  were higher in winter followed by summer, spring and the lowest in autumn (Table  
539 1). Annual and seasonal averages of FI values of both  $WSBrC$  and  $WI-MSBrC$  were around or  
540 higher than 1.4 and lower than 1.9 in Tianjin, indicating that the BrC in Tianjin was mainly derived  
541 from terrestrial OM that should have largely consist of high aromatic compounds. In contrast, the  
542 annual and seasonal averages of BIX of both  $WSBrC$  and  $WI-MSBrC$  were higher than 1.0 (Table  
543 1), indicating the predominant contributions of OM from the biological (including biomass  
544 burning) sources. In addition, the lowest  $FI_{WSBrC}$  and  $BIX_{WSBrC}$  values in summer and those of the  
545  $FI_{WI-MSBrC}$  in spring and  $BIX_{WI-MSBrC}$  in autumn suggest that the contribution from terrestrial  
546 sources (e.g., coal combustion) might be less in spring and autumn and the photobleaching of OA  
547 might be significant under high solar radiation in summer.

548  $HIX_{WSBrC}$  and  $HIX_{WI-MSBrC}$  were ranged from 1.72 to 4.7 with an average of 2.87 and  
549 0.11-2.38 (avg. 0.81), respectively, during the campaign, which again support that both the BrC  
550 components in Tianjin should have been significantly derived from biomass burning and might  
551 consist highly humified and aromatic compounds. Average  $HIX_{WSBrC}$  was higher in summer  
552 followed by autumn, spring and the lowest in winter (Table 1). In contrast, the average  $HIX_{WI-MSBrC}$   
553 was higher in winter followed by autumn, spring and the lowest in summer (Table 1). It has  
554 been reported that aging processes and HIX have a significant relation (Deng et al., 2022). The  
555 higher  $HIX_{WSBrC}$  and lower  $HIX_{WI-MSBrC}$  in summer confirm that the BrC, which is more water-  
556 soluble, was significantly produced from aromatic compounds and subjected for significant  
557 atmospheric aging in summer over the Tianjin region.

558





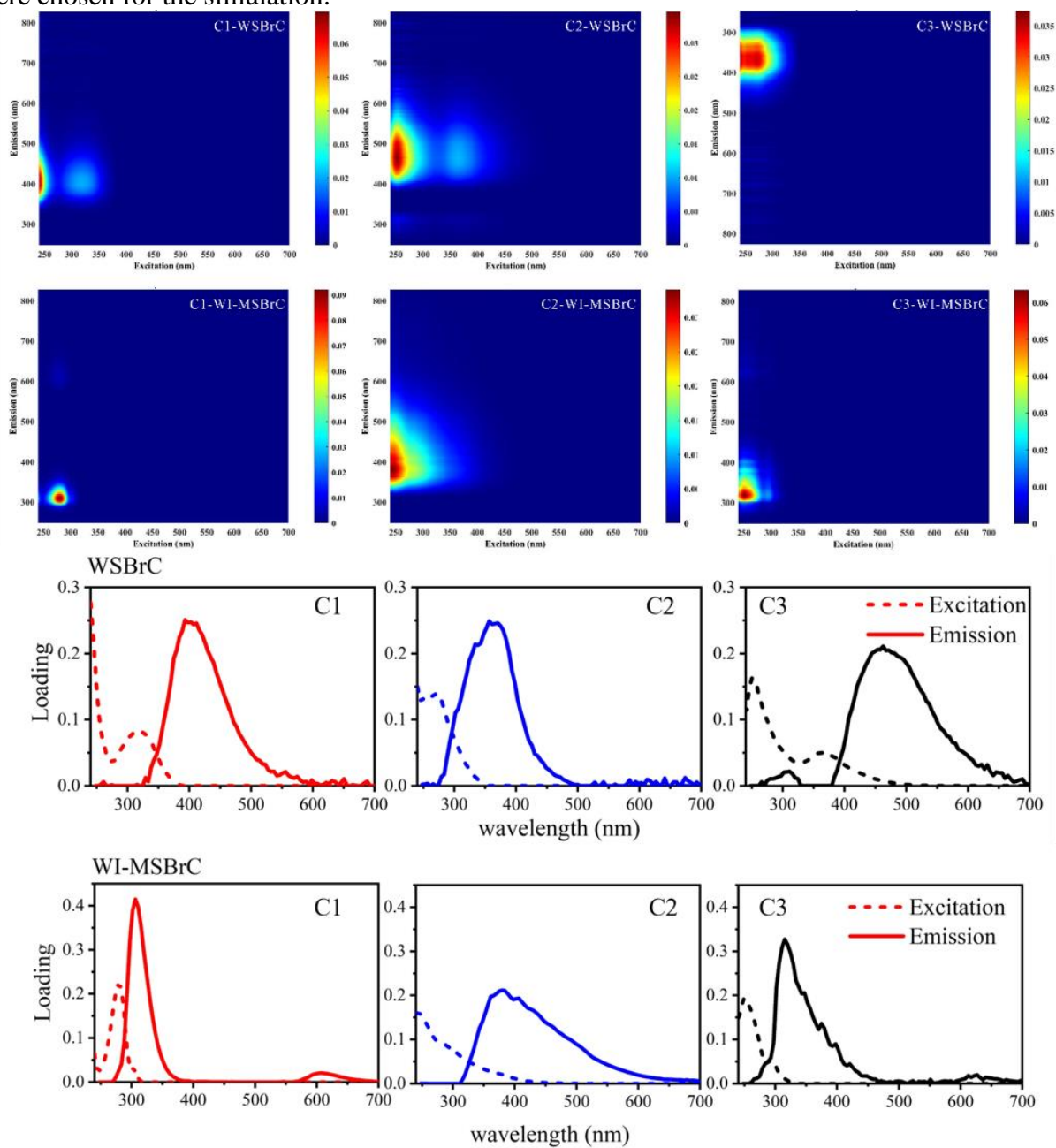
559

560 **Figure 4.** Temporal variations in light absorption and fluorescence properties of BrC in PM<sub>2.5</sub>  
 561 Tianjin: (a) FI, (b) BIX, and (c) HIX.

562 3.3.2 Fluorophore identification

563 It is well established that fluorophores with different excitation emission wavelengths can  
 564 distinguish their types and sources. However, the types and sources of a large number of  
 565 fluorophores have not been determined due to their complex chemical composition and sources.  
 566 Here, we separated several fluorescence components from the EEM data using the parallel factor  
 567 analysis (PARAFAC) model, and the results are shown in Fig. 5. The fact of the value of core  
 568 consistency close to 100 in PARAFAC model indicates that the more the individual components

569 that are analyzed together make up 100% of the mixture, with no unexplained residues. The core  
 570 consistency of PARAFAC model explained the maximum variance of 89% for WSBrc and of  
 571 95% for WI-MSBrC whole data obtained during the campaign, when three independent groups  
 572 were chosen for the simulation.



573  
 574 **Figure 5.** Three-dimensional excitation-emission matrix of three fluorescent components with  
 575 emission in WSBrc (above) and WI-MSBrC (below) obtained by PARAFAC model analysis.

576 The types of fluorophores of both WSBrc and WI-MSBrC identified in this study together  
 577 with their excitation and emission wavelengths and those reported in the literature are summarized  
 578 in Table 2. Among the total of three types of fluorophores obtained for WSBrc in Tianjin PM<sub>2.5</sub>

579 by PARAFAC for EEMs, two showed the fluorescence characteristics similar to those of less  
 580 oxygenated and highly oxygenated humic-like substances (HULIS), respectively, and the third one  
 581 showed similar to those of protein compounds (PLOM). Fluorophore C1<sub>WSBrC</sub> has a primary  
 582 fluorescence peak at excitation/emission (Ex/Em): <240/393 nm, and a secondary fluorescence  
 583 peak at Ex/Em: 318/393 nm. C1<sub>WSBrC</sub> can be classified as a humus-like fluorophore because the  
 584 bimodal distribution of the fluorescence spectrum is usually associated with HULIS. The emission  
 585 wavelength of C1<sub>WSBrC</sub> was closer to the UV region than that of the second peak of C2<sub>WSBrC</sub>,  
 586 indicating the existence of a small number of aromatic substances, conjugate systems and  
 587 nonlinear ring systems (Deng et al., 2022). C2<sub>WSBrC</sub> (Ex/Em ~251, 363 nm/462 nm) was identified  
 588 as a common HULIS in aerosols, with higher oxidation, aromatization, molecular weight,  
 589 conjugation, and unsaturation due to its larger emission wavelength (Wen et al., 2021). The  
 590 molecular weight of the fluorophore as well as its degree of conjugation tend to increase with the  
 591 excitation wavelength, and such increase in size and the conjugation degree may be attributed to  
 592 the presence of highly aromatic conjugated structures containing heteroatoms (Chen et al., 2019).  
 593 Compared to C1<sub>WSBrC</sub> and C2<sub>WSBrC</sub>, C3<sub>WSBrC</sub> also contains two peaks, with shorter wavelengths  
 594 (<380 nm) emission peak, which is usually associated with protein-like organic matter (PLOM)  
 595 such as tryptophan and tyrosine, with low aromatic properties and small molecular size (Table 2).

597 **Table 2.** Description and wavelength positions of PARAFAC components in this study and other  
 598 reports from the literature. (PLOM = protein compounds; HULIS = humic-like substances)

Category	Components	Ex(nm)	Em(nm)	Substances	References
WSBrC	C1	<240, 318	393	low-oxygenated HULIS	this study
	C2	251, 363	462	high-oxygenated HULIS	
	C3	<240, 271	356.3	PLOM, such as tryptophan and tyrosine	
WI-MSBrC	C1	<240, 279	306	PLOM, tyrosine-like	
	C2	<240	379	uncertain	
	C3	251, 294	315	PLOM, tryptophan-like	
Water-soluble BrC	C1	250, 315	396	low-oxygenated HULIS	(Deng et al., 2022)
	C2	250	465	highly-oxygenated HULIS	
	C3	250	385	low-oxygenated HULIS	
	C4	250	340	PLOM, tryptophan-like	
	C5	275	305	PLOM, tyrosine-like	
WSOC	C1	240, 315	393	low-oxygenated HULIS	(Wen et al., 2021)
	C2	245, 360	476	highly-oxygenated HULIS	
	C3	<240, 290	361	PLOM, such as tryptophan and tyrosine	
	C4	275	311	PLOM, tyrosine-like	
WSM and MSM	C1	255	415	HULIS-1 component	(Chen et al., 2019)
	C2	220	340	tryptophan-like component	
	C3	255	385	HULIS-2 component	
	C4	210	300	tyrosine-like component	
	C5	250	355	amino acid-like component	
WSOC	C1	245	410	HULIS, photodegradation of macromolecules	(Xie et al., 2020)
	C2	235	398	HULIS, aromatic and saturated compounds were presented	
	C3	250, 360	466	humic-like chromophores, more aromatic and consisted of more unsaturated compounds produced by condensation reactions	
	C4	250, 285	432	terrestrial humic-like chromophore	
	C5	<235	430	terrestrial humic-like substance, photochemical product	
MSOC	C6	275	408	low oxidation humic-like	
	C7	235, 275	372	protein-like chromophore	
	C8	260, 310	364	protein-like (tryptophan-like), may be related to PAHs	

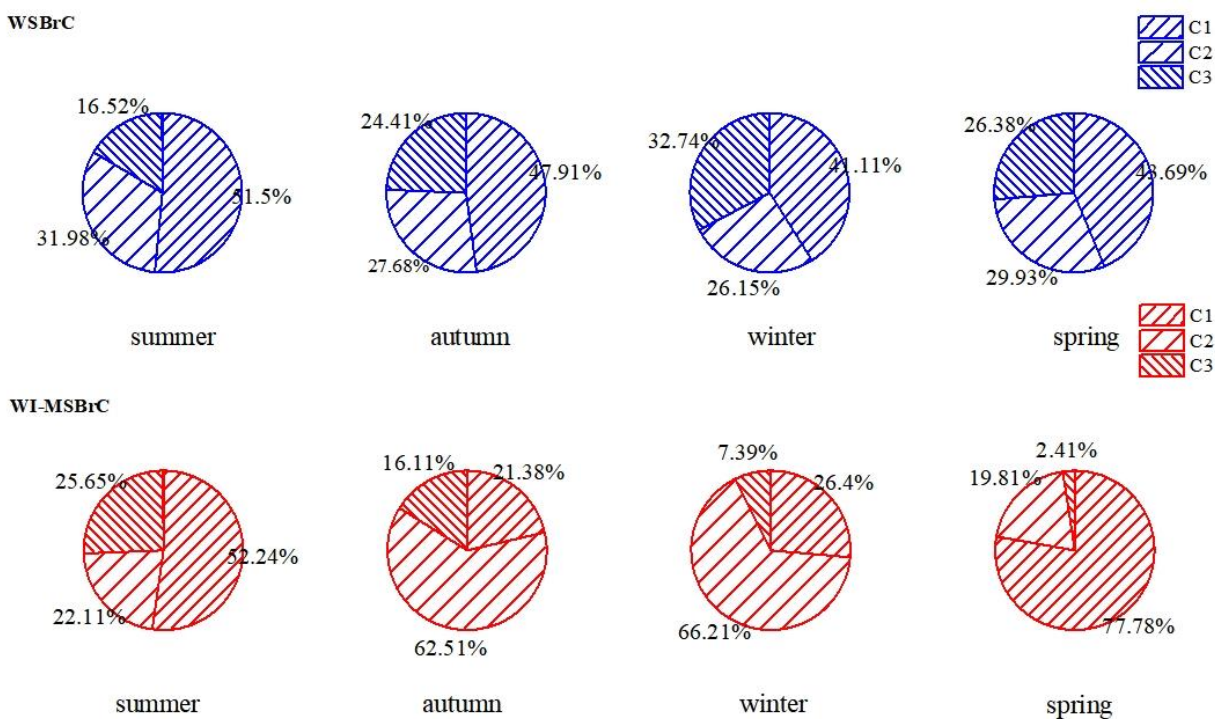
599  
 600 However, WI-MSBrC fluorophore C1<sub>WI-MSBrC</sub> might be tyrosine-like substance. C2<sub>WI-MSBrC</sub>  
 601 is not quite certain and could be either HULIS or PLOM, because its emission wavelength <380

602 nm generally fits the profile of PLOM, but it is also close to the emission wavelength of HULIS.  
 603 While C3<sub>WI-MSBrC</sub> is a tryptophan-like substance, which was reported to contain less aromatic and  
 604 small molecular weight compounds. In general, phenols contribute significantly to C3<sub>WI-MSBrC</sub>  
 605 fluorophore as they are the products of incomplete pyrolysis of lignin and cellulose and are used  
 606 as indicators of biomass burning (Wen et al., 2021). Therefore, WI-MSBrC fluorophores of all  
 607 samples in this study can be classified as mainly PLOM.

608 The percent contributions of each fluorophore to WSB<sub>rC</sub> and WI-MSBrC in PM<sub>2.5</sub> in Tianjin  
 609 in each season are shown in Fig. 6. The compositions of WSB<sub>rC</sub> and WI-BrC clearly imply that  
 610 the former contained more HULIS, whereas the later consist mostly of PLOM, and also indicate  
 611 that most of the fluorophores of protein-like substances could dissolve in organic solvent, rather  
 612 than in water.

613 According to the excitation emission wavelength, we classified the fluorescence component  
 614 of WI-MSBrC substance as PLOM, but the correlation between their fluorescence intensity and  
 615 BIX ( $R = 0.66, p < 0.05$ ) was very small, far lower than that of WSB<sub>rC</sub> substance and BIX ( $R =$   
 616  $0.59, p < 0.05$ ). On the contrary, the correlation between their fluorescence intensity and HIX ( $R =$   
 617  $0.74, p < 0.05$ ) was much higher than that of WSB<sub>rC</sub> ( $R = -0.10, p < 0.05$ ). Although PLOM  
 618 may be associated with some polycyclic aromatic hydrocarbons (PAHs) or phenols from fossil  
 619 fuel combustion and biomass burning, especially in urban aerosols, the correlation is puzzling.

620



621

622 **Figure 6.** Relative abundances of the chromophores of the WSB<sub>rC</sub> and WI-MSBrC in PM<sub>2.5</sub>  
 623 from Tianjin.

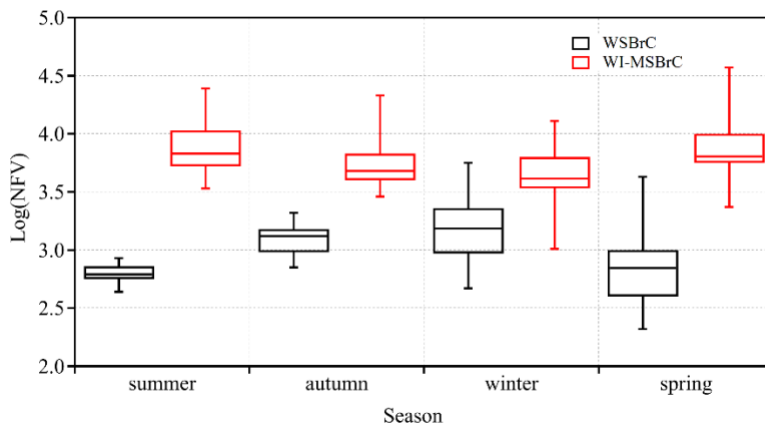
624 On average, the humic-like fluorophores together contributed more than 60% to the  
 625 fluorescence intensity in WSB<sub>rC</sub>, suggesting that humic-like fluorophores played a dominant role  
 626 in fluorescence properties of WSB<sub>rC</sub> in Tianjin. Generally, the low-oxygenated fluorophores  
 627 C1<sub>WSBrC</sub> made considerable contributions in each season. While C2<sub>WSBrC</sub>, highly oxygenated

628 HULIS, has a greater relative contribution in summer, which might be due to the strong solar  
629 radiation in summer. In contrast, in WI-MSBrC, the average contribution of PLOM to fluorescence  
630 intensity was higher than 70% in spring (80.2%) and summer (77.9%), but C2<sub>WI-MSBrC</sub> component  
631 dominated in winter and autumn. This indicated that biological activities increased in spring and  
632 summer and the relative abundance of bioaerosols might be higher during that period.

### 633 3.4 Potential sources of BrC

634 To further explore the potential sources of BrC, correlations of FV with chemical components  
635 and light absorption of PM<sub>2.5</sub> were examined. The sum of FVs of WSBrc and WI-MSBrC  
636 (FV<sub>S(WSBrc+WI-MSBrC)</sub>) showed a significant correlation with secondary OC (SOC) in autumn ( $R =$   
637  $0.90, p < 0.05$ ) and winter ( $R = 0.67, p < 0.05$ ). Furthermore, the correlation between FV<sub>S(WSBrc+WI-</sub>  
638 <sub>MSBrC)</sub> and EC in each season was insignificant. Such relations suggest that the secondary  
639 formation processes should have been played an important role in controlling the loadings of BrC  
640 in autumn and winter as well. A good correlation between FV and Abs<sub>365</sub> of both WSBrc and WI-  
641 MSBrC was found in all seasons except winter, which indicates that most light-absorbing materials  
642 would also have significant fluorescence characteristics.

643 The relative contents of different chromophores in different polar extracts depend on their  
644 sources and varied significantly. The results showed that the NFVs of WSBrc were lower than  
645 those the WI-MSBrC and were different from season to season in Tianjin (Fig. 7). Recently, it has  
646 been reported that the aerosols derived from biomass burning and coal combustion exhibit the  
647 highest NFV values, while SOA show the lowest NFV values (Chen et al., 2020). NFV in all  
648 samples studied in Tianjin during 2018–2019 was very similar to that of primary emissions and  
649 higher than that of secondary aerosols. Such result reveal that the fluorophores in the Tianjin PM<sub>2.5</sub>  
650 might mainly be derived from a primary combustion sources as well. In addition, the NFVs of the  
651 Tianjin PM<sub>2.5</sub> were higher in winter than in summer, which is likely and can be attributed to the  
652 photolysis of chromophores in summer. In addition, NFV of WI-MSBrC was much higher than  
653 that in WSBrc, which indicate that fluorescence contribution of fluorophores was abundant in WI-  
654 MSBrC than in the WSBrc.



655  
656 **Figure 7.** The normalized fluorescence volumes (NFVs) of the WSBrc and WI-MSBrC of PM<sub>2.5</sub>  
657 from Tianjin, North China.

658

#### 659 **4. Summary and Conclusions**

660 This study presents the temporal variations in light absorption and fluorescence properties of  
661 water-soluble BrC (WSBrC) and the water-insoluble but MeOH-soluble BrC (WI-MSBrC) in  
662 PM<sub>2.5</sub> collected from Tianjin, North China during July 5, 2018 – July 5, 2019. Light absorption  
663 properties of WSBrC and WI-MSBrC in Tianjin were investigated and found to be distinct from  
664 season to season, which was lower in spring and summer, compared with that in autumn and  
665 winter. The AAE of WI-MSBrC was comparable with that of WSBrC. The mass absorption  
666 efficiency of WSBrC and WI-MSBrC (MAE<sub>365</sub>) exhibited distinct seasonal variations, which was  
667 higher in winter and lower in summer and autumn. Biologically derived or secondary BrC and/or  
668 its photobleaching might be the reasons for the lower MAE<sub>365</sub> values in summer and autumn. The  
669 light absorption of both WSBrC and WI-MSBrC in the range of 300–400 nm to that in the whole  
670 range (300–700 nm) was ~40%, indicating that BrC in the UV-Vis range plays an important role  
671 in climate warming. In addition, based on PARAFAC analysis model, EEM data were  
672 comprehensively analyzed to identify the types and abundance of different fluorophores, and  
673 obtained three types of the fluorophores: low-oxygenated HULIS, high-oxygenated HULIS and  
674 protein-like compound (PLOM). The correlation between BrC optical properties and aerosol  
675 chemical composition indicated that biomass burning, and fossil fuel (mainly coal) combustion  
676 significantly contributed to BrC content in winter, while primary biological emission and  
677 subsequent aging significantly contributed to the BrC content in summer. These results illustrated  
678 the light absorption properties of BrC in metropolis aerosols and emphasized its significant  
679 contribution to radiative forcing.

#### 680 **Declaration of competing interest**

681 The authors declare no competing interest in this paper.

#### 682 **Data Availability Statement**

683 The data used in this study can be found online at <https://doi.org/10.5281/zenodo.7316371> (Dong  
684 et al., 2022), and at <https://doi.org/10.5281/zenodo.5140861> (Dong et al., 2021).

#### 685 **Supplement.**

686 The supplement related to this article is available online at:

#### 687 **Acknowledgments**

688 This work was supported in part by National Natural Science Foundation of China (Grant No.  
689 41775120 and 42277090) & National Key Research and Development Plan (Grant No.  
690 2017YFC0212700), China. The author also thanks to Mr. Yunting Xiao's help for writing a code  
691 to calculate the SFE.

#### 692 **Author contribution**

693 ZD and CMP conceptualized this study. ZD and PL conducted the sampling. ZD conducted the

694 chemical analyses, interpreted the data and wrote the manuscript. CMP supervised the research  
695 and acquired the funding for this study. XZ, ZXY and ZXJ administrated the project. CMP, ZX,  
696 DJ, PF and CQL contributed in discussing the results and review and editing the manuscript.

## 697 **References**

- 698 Andreae, M. O., and Gelencsér, A.: Black carbon or brown carbon? The nature of light-absorbing carbonaceous  
699 aerosols, *Atmospheric Chemistry and Physics*, 6, 3131–3148, [www.atmos-chem-phys.net/6/3131/2006/](http://www.atmos-chem-phys.net/6/3131/2006/), 2006.
- 700 Baduel, C., Voisin, D., and Jaffrezo, J. L.: Comparison of analytical methods for Humic Like Substances (HULIS)  
701 measurements in atmospheric particles, *Atmospheric Chemistry and Physics*, 9, 5949–5962, 10.5194/acp-9-5949-  
702 2009, 2009.
- 703 Battin, T. J.: Dissolved organic matter and its optical properties in a blackwater tributary of the upper Orinoco river,  
704 Venezuela, *Organic Geochemistry*, 28, 561–569, [https://doi.org/10.1016/S0146-6380\(98\)00028-X](https://doi.org/10.1016/S0146-6380(98)00028-X), 1998.
- 705 Birdwell, J. E., and Engel, A. S.: Characterization of dissolved organic matter in cave and spring waters using UV-  
706 Vis absorbance and fluorescence spectroscopy, *Org Geochem*, 41, 270–280, 10.1016/j.orggeochem.2009.11.002,  
707 2010.
- 708 Bond, T. C., and Bergstrom, R. W.: Light absorption by carbonaceous particles: An investigative review, *Aerosol*  
709 *Science and Technology*, 40, 27–67, 10.1080/02786820500421521, 2006.
- 710 Brown, H., Liu, X., Pokhrel, R., Murphy, S., Lu, Z., Saleh, R., Mielonen, T., Kokkola, H., Bergman, T., Myhre, G.,  
711 Skeie, R. B., Watson-Paris, D., Stier, P., Johnson, B., Bellouin, N., Schulz, M., Vakkari, V., Beukes, J. P., van Zyl,  
712 P. G., Liu, S., and Chand, D.: Biomass burning aerosols in most climate models are too absorbing, *Nature*  
713 *Communications*, 12, 277, 10.1038/s41467-020-20482-9, 2021.
- 714 Cao, T., Li, M., Xu, C., Song, J., Fan, X., Li, J., Jia, W., and Peng, P.: Technical note: Identification of chemical  
715 composition and source of fluorescent components in atmospheric water-soluble brown carbon by excitation-  
716 emission matrix with parallel factor analysis: Potential limitation and application, *Atmospheric Chemistry and*  
717 *Physics Discussions*, 2022, 1–41, 10.5194/acp-2022-676, 2022.
- 718 Chen, Q., Fumikazu, I., Hayato, H., Daichi, A., and Michihiro, M.: Chemical structural characteristics of HULIS  
719 and other fractionated organic matter in urban aerosols: Results from mass spectral and FT-IR analysis,  
720 *Environmental Science & Technology*, 50, 1721–1730, 10.1021/acs.est.5b05277, 2016a.
- 721 Chen, Q., Miyazaki, Y., Kawamura, K., Matsumoto, K., Coburn, S., Volkamer, R., Iwamoto, Y., Kagami, S., Deng,  
722 Y., Ogawa, S., Ramasamy, S., Kato, S., Ida, A., Kajii, Y., and Mochida, M.: Characterization of chromophoric  
723 water-soluble organic matter in urban, forest, and marine aerosols by HR-ToF-AMS analysis and excitation-  
724 emission matrix spectroscopy, *Environmental Science & Technology*, 50, 10351–10360, 10.1021/acs.est.6b01643,  
725 2016b.
- 726 Chen, Q., Mu, Z., Song, W., Wang, Y., Yang, Z., Zhang, L., and Zhang, Y.-L.: Size-resolved characterization of the  
727 chromophores in atmospheric particulate matter from a typical coal-burning city in China, *Journal of Geophysical*  
728 *Research: Atmospheres*, 124, 10546–10563, <https://doi.org/10.1029/2019JD031149>, 2019.
- 729 Chen, Q., Li, J., Hua, X., Jiang, X., Mu, Z., Wang, M., Wang, J., Shan, M., Yang, X., Fan, X., Song, J., Wang, Y.,  
730 Guan, D., and Du, L.: Identification of species and sources of atmospheric chromophores by fluorescence excitation-  
731 emission matrix with parallel factor analysis, *Science of the Total Environment*, 718, 137322,  
732 10.1016/j.scitotenv.2020.137322, 2020.
- 733 Chen, Q. C., Ikemori, F., and Mochida, M.: Light Absorption and Excitation-Emission Fluorescence of Urban  
734 Organic Aerosol Components and Their Relationship to Chemical Structure, *Environ Sci Technol*, 50, 10859–10868,  
735 10.1021/acs.est.6b02541, 2016c.
- 736 Choudhary, V., Rajput, P., and Gupta, T.: Absorption properties and forcing efficiency of light-absorbing water-  
737 soluble organic aerosols: Seasonal and spatial variability, *Environ Pollut*, 272, ARTN 115932  
738 10.1016/j.envpol.2020.115932, 2021.
- 739 Coble, P. G.: Marine optical biogeochemistry: The chemistry of ocean color, *Chem Rev*, 107, 402–418,  
740 10.1021/cr050350+, 2007.
- 741 Corbin, J. C., Czech, H., Massabò, D., de Mongeot, F. B., Jakobi, G., Liu, F., Lobo, P., Mennucci, C., Mensah, A.  
742 A., Orasche, J., Pieber, S. M., Prévôt, A. S. H., Stengel, B., Tay, L. L., Zanatta, M., Zimmermann, R., El Haddad, I.,  
743 and Gysel, M.: Infrared-absorbing carbonaceous tar can dominate light absorption by marine-engine exhaust, *npj*  
744 *Climate and Atmospheric Science*, 2, 12, 10.1038/s41612-019-0069-5, 2019.

745 Deng, J., Ma, H., Wang, X., Zhong, S., Zhang, Z., Zhu, J., Fan, Y., Hu, W., Wu, L., Xiaodong, L., Ren, L., Pavuluri,  
746 C. M., Pan, X., Sun, Y., Wang, Z., Kawamura, K., and Fu, P.: Measurement Report: Optical properties and sources  
747 of water-soluble brown carbon in Tianjin, North China: insights from organic molecular compositions, *Atmospheric  
748 Chemistry and Physics*, 22, 6449-6470, 10.5194/acp-2021-1045, 2022.

749 Diggs, D. L., Huderson, A. C., Harris, K. L., Myers, J. N., Banks, L. D., Rekhadevi, P. V., Niaz, M. S., and Ramesh,  
750 A.: Polycyclic aromatic hydrocarbons and digestive tract cancers: a perspective, *Journal of Environmental Science  
751 and Health, Part C*, 29, 324-357, 10.1080/10590501.2011.629974, 2011.

752 Dong, Z., Pavuluri, C. M., Xu, Z., Wang, Y., Li, P., Fu, P., and Liu, C. Q.: Measurement report: Chemical  
753 components and <sup>13</sup>C and <sup>15</sup>N isotope ratios of fine aerosols over Tianjin, North China: year-round observations,  
754 *Atmospheric Chemistry and Physics*, 23, 2119-2143, 10.5194/acp-23-2119-2023, 2023a.

755 Dong, Z. C., Pavuluri, C. M., Xu, Z. J., Wang, Y., Li, P. S., Fu, P. Q., and Liu, C. Q.: Year-round observations of  
756 bulk components and <sup>13</sup>C and <sup>15</sup>N isotope ratios of fine aerosols at Tianjin, North China – Data set. 2021.

757 Dong, Z. C., Pavuluri, C. M., Li, P. S., Xu, Z. J., Deng, J. J., Zhao, X. Y., and Zhao, X. M.: Year-round observations  
758 of the optical properties of brown carbon in fine aerosols at Tianjin, North China – Data set. 2022.

759 Dong, Z. C., Pavuluri, C. M., Xu, Z. J., Wang, Y., Li, P. S., Fu, P. Q., and Liu, C. Q.: Measurement report:  
760 Chemical components and  
761 C and  
762 N isotoperatios of fine aerosols over Tianjin, North China: year-round observations, *Atmos Chem Phys*, 23, 2119-  
763 2143, 10.5194/acp-23-2119-2023, 2023b.

764 Fan, X. J., Wei, S. Y., Zhu, M. B., Song, J. Z., and Peng, P. A.: Comprehensive characterization of humic-like  
765 substances in smoke PM  
766 emitted from the combustion of biomass materials and fossil fuels, *Atmos Chem Phys*, 16, 13321-13340,  
767 10.5194/acp-16-13321-2016, 2016.

768 Feng, Y., Ramanathan, V., and Kotamarthi, V. R.: Brown carbon: a significant atmospheric absorber of solar  
769 radiation?, *Atmospheric Chemistry and Physics Discussions*, 10.5194/acpd-13-2795-2013, 2013.

770 Gao yan, and Zhang, y.: Formation and photochemical investigation of brown carbon by hydroxyacetone reactions  
771 with glycine and ammonium sulfate, *Royal Society of Chemistry Advances*, 8, 20719-20725,  
772 10.1039/C8RA02019A, 2018.

773 Gu, Q., and Kenny, J. E.: Improvement of inner filter effect correction based on determination of effective geometric  
774 parameters using a conventional fluorimeter, *Analytical Chemistry*, 81, 420-426, 10.1021/ac801676j, 2009.

775 Hecobian, A., Zhang, X., Zheng, M., Frank, N., Edgerton, E. S., and Weber, R. J.: Water-Soluble Organic Aerosol  
776 material and the light-absorption characteristics of aqueous extracts measured over the Southeastern United States,  
777 *Atmospheric Chemistry and Physics*, 10, 5965-5977, 10.5194/acp-10-5965-2010, 2010.

778 Hems, R. F., Schnitzler, E. G., Liu-Kang, C., Cappa, C. D., and Abbatt, J. P. D.: Aging of atmospheric brown carbon  
779 aerosol, *ACS Earth and Space Chemistry*, 5, 722-748, 10.1021/acsearthspacechem.0c00346, 2021.

780 Hoffer, A., Gelencsér, A., Guyon, P., Kiss, G., Schmid, O., Frank, G. P., Artaxo, P., and Andreae, M. O.: Optical  
781 properties of humic-like substances (HULIS) in biomass-burning aerosols, *Atmospheric Chemistry and Physics*, 6,  
782 3563-3570, 10.5194/acp-6-3563-2006, 2006.

783 Huang, R. J., Yang, L., Cao, J., Chen, Y., Chen, Q., Li, Y., Duan, J., Zhu, C., Dai, W., Wang, K., Lin, C., Ni, H.,  
784 Corbin, J. C., Wu, Y., Zhang, R., Tie, X., Hoffmann, T., O'Dowd, C., and Dusek, U.: Brown carbon aerosol in urban  
785 Xi'an, Northwest China: The composition and light absorption properties, *Environmental Science & Technology*,  
786 52, 6825-6833, 10.1021/acs.est.8b02386, 2018.

787 Huang, R. J., Yang, L., Shen, J., Yuan, W., Gong, Y., Guo, J., Cao, W., Duan, J., Ni, H., Zhu, C., Dai, W., Li, Y.,  
788 Chen, Y., Chen, Q., Wu, Y., Zhang, R., Dusek, U., O'Dowd, C., and Hoffmann, T.: Water-insoluble organics  
789 dominate brown carbon in wintertime urban aerosol of China: Chemical characteristics and optical properties,  
790 *Environmental Science & Technology*, 54, 7836-7847, 10.1021/acs.est.0c01149, 2020.

791 Jo, D. S., Park, R. J., Lee, S., Kim, S. W., and Zhang, X.: A global simulation of brown carbon: implications for  
792 photochemistry and direct radiative effect, *Atmospheric Chemistry and Physics*, 16, 3413-3432, 10.5194/acp-16-  
793 3413-2016, 2016.

794 Kasthuriarachchi, N. Y., Rivellini, L.-H., Chen, X., Li, Y. J., and Lee, A. K. Y.: Effect of relative humidity on  
795 secondary brown carbon formation in aqueous droplets, *Environmental Science & Technology*, 54, 13207-13216,  
796 10.1021/acs.est.0c01239, 2020.

797 Lack, D. A., Bahreni, R., Langridge, J. M., Gilman, J. B., and Middlebrook, A. M.: Brown carbon absorption linked  
798 to organic mass tracers in biomass burning particles, *Atmospheric Chemistry and Physics*, 13, 2415-2422,  
799 10.5194/acp-13-2415-2013, 2013.



800 Laskin, A., Laskin, J., and Nizkorodov, S. A.: Chemistry of Atmospheric Brown Carbon, *Chem Rev*, 115, 4335-  
801 4382, 10.1021/cr5006167, 2015a.

802 Laskin, A., Laskin, J., and Nizkorodov, S. A.: Chemistry of atmospheric brown carbon, *Chemical Reviews*, 115,  
803 4335-4382, 10.1021/cr5006167, 2015b.

804 Lawaetz, A. J., and Stedmon, C. A.: Fluorescence intensity calibration using the Raman scatter peak of water,  
805 *Applied Spectroscopy*, 63, 936-940, 10.1366/000370209788964548, 2009.

806 Lee, H. J., Laskin, A., Laskin, J., and Nizkorodov, S. A.: Excitation-Emission Spectra and Fluorescence Quantum  
807 Yields for Fresh and Aged Biogenic Secondary Organic Aerosols, *Environ Sci Technol*, 47, 5763-5770,  
808 10.1021/es400644c, 2013.

809 Lesworth, T., Baker, A. R., and Jickells, T.: Aerosol organic nitrogen over the remote Atlantic Ocean, *Atmospheric*  
810 *Environment*, 44, 1887-1893, <https://doi.org/10.1016/j.atmosenv.2010.02.021>, 2010.

811 Li, C., He, Q., Hettiyadura, A. P. S., Käfer, U., Shmul, G., Meidan, D., Zimmermann, R., Brown, S. S., George, C.,  
812 Laskin, A., and Rudich, Y.: Formation of secondary brown carbon in biomass burning aerosol proxies through NO<sub>3</sub>  
813 radical reactions, *Environmental Science & Technology*, 54, 1395-1405, 10.1021/acs.est.9b05641, 2020a.

814 Li, J., Zhang, Q., Wang, G., Li, J., Wu, C., Liu, L., Wang, J., Jiang, W., Li, L., Ho, K. F., and Cao, J.: Optical  
815 properties and molecular compositions of water-soluble and water-insoluble brown carbon (BrC) aerosols in  
816 northwest China, *Atmospheric Chemistry and Physics*, 20, 4889-4904, 10.5194/acp-20-4889-2020, 2020b.

817 Li, S., Zhu, M., Yang, W. Q., Tang, M. J., Huang, X. L., Yu, Y. G., Fang, H., Yu, X., Yu, Q. Q., Fu, X. X., Song,  
818 W., Zhang, Y. L., Bi, X. H., and Wang, X. M.: Filter-based measurement of light absorption by brown carbon in  
819 PM<sub>2.5</sub> in a megacity in South China, *Science of the Total Environment*, 633, 1360-1369,  
820 10.1016/j.scitotenv.2018.03.235, 2018.

821 Li, X., Fu, P., Tripathee, L., Yan, F., Hu, Z., Yu, F., Chen, Q., Li, J., Chen, Q., Cao, J., and Kang, S.: Molecular  
822 compositions, optical properties, and implications of dissolved brown carbon in snow/ice on the Tibetan Plateau  
823 glaciers, *Environment International*, 164, 107276, <https://doi.org/10.1016/j.envint.2022.107276>, 2022.

824 Liakakou, E., Kaskaoutis, D. G., Grivas, G., Stavroulas, I., Tsagkaraki, M., Paraskevopoulou, D., Bougiatioti, A.,  
825 Dumka, U. C., Gerasopoulos, E., and Mihalopoulos, N.: Long-term brown carbon spectral characteristics in a  
826 Mediterranean city (Athens), *Sci Total Environ*, 708, 135019, 10.1016/j.scitotenv.2019.135019, 2020.

827 Lin, G., Penner, J. E., Flanner, M. G., Sillman, S., Xu, L., and Zhou, C.: Radiative forcing of organic aerosol in the  
828 atmosphere and on snow: Effects of SOA and brown carbon, *Journal of Geophysical Research: Atmospheres*, 119,  
829 7453-7476, 10.1002/2013jd021186, 2014.

830 Lin, P., Bluvshstein, N., Rudich, Y., Nizkorodov, S. A., Laskin, J., and Laskin, A.: Molecular Chemistry of  
831 Atmospheric Brown Carbon Inferred from a Nationwide Biomass Burning Event, *Environ Sci Technol*, 51, 11561-  
832 11570, 10.1021/acs.est.7b02276, 2017.

833 Liu, J., Bergin, M., Guo, H., King, L., Kotra, N., Edgerton, E., and Weber, R. J.: Size-resolved measurements of  
834 brown carbon in water and methanol extracts and estimates of their contribution to ambient fine-particle light  
835 absorption, *Atmospheric Chemistry and Physics*, 13, 12389-12404, 10.5194/acp-13-12389-2013, 2013.

836 McKnight, D. M., Boyer, E. W., Westerhoff, P. K., Doran, P. T., Kulbe, T., and Andersen, D. T.:  
837 Spectrofluorometric Characterization of Dissolved Organic Matter for Indication of Precursor Organic Material and  
838 Aromaticity, *Limnology and Oceanography*, 46, 38-48, 2001.

839 Murphy, K. R., Stedmon, C. A., Graeber, D., and Bro, R.: Fluorescence spectroscopy and multi-way techniques.  
840 PARAFAC, *Analytical Methods*, 5, 6557-6566, 10.1039/C3AY41160E, 2013.

841 Park, R. J., Kim, M. J., Jeong, J. I., Youn, D., and Kim, S.: A contribution of brown carbon aerosol to the aerosol  
842 light absorption and its radiative forcing in East Asia, *Atmospheric Environment*, 44, 1414-1421,  
843 10.1016/j.atmosenv.2010.01.042, 2010.

844 Peters, S., Talaska, G., Jonsson, B. A., Kromhout, H., and Vermeulen, R.: Polycyclic aromatic hydrocarbon  
845 exposure, urinary mutagenicity, and DNA adducts in rubber manufacturing workers, *Cancer Epidemiol Biomarkers*  
846 *Prev*, 17, 1452-1459, 10.1158/1055-9965.EPI-07-2777, 2008.

847 Qin, J., Zhang, L., Zhou, X., Duan, J., Mu, S., Xiao, K., Hu, J., and Tan, J.: Fluorescence fingerprinting properties  
848 for exploring water-soluble organic compounds in PM<sub>2.5</sub> in an industrial city of northwest China, *Atmospheric*  
849 *Environment*, 184, 203-211, <https://doi.org/10.1016/j.atmosenv.2018.04.049>, 2018.

850 Rizzo, L. V., Correia, A. L., Artaxo, P., Procópio, A. S., and Andreae, M. O.: Spectral dependence of aerosol light  
851 absorption over the Amazon Basin, *Atmospheric Chemistry and Physics*, 11, 8899-8912, 10.5194/acp-11-8899-  
852 2011, 2011.

853 Rizzo, L. V., Artaxo, P., Müller, T., Wiedensohler, A., Paixão, M., Cirino, G. G., Arana, A., Swietlicki, E., Roldin,  
854 P., Fors, E. O., Wiedemann, K. T., Leal, L. S. M., and Kulmala, M.: Long term measurements of aerosol optical

855 properties at a primary forest site in Amazonia, *Atmos. Chem. Phys.*, 13, 2391-2413, 10.5194/acp-13-2391-2013,  
856 2013.

857 Saleh, R.: From Measurements to Models: Toward Accurate Representation of Brown Carbon in Climate  
858 Calculations, *Current Pollution Reports*, 6, 90-104, 10.1007/s40726-020-00139-3, 2020.

859 Shamjad, P. M., Tripathi, S. N., Thamban, N. M., and Vreeland, H.: Refractive Index and Absorption Attribution of  
860 Highly Absorbing Brown Carbon Aerosols from an Urban Indian City-Kanpur, *Sci Rep-Uk*, 6, 10.1038/srep37735,  
861 2016.

862 Shetty, N. J., Pandey, A., Baker, S., Hao, W. M., and Chakrabarty, R. K.: Measuring light absorption by freshly  
863 emitted organic aerosols: optical artifacts in traditional solvent-extraction-based methods, *Atmos. Chem. Phys.*, 19,  
864 8817-8830, 10.5194/acp-19-8817-2019, 2019.

865 Sun, J., Zhi, G., Hitznerberger, R., Chen, Y., Tian, C., Zhang, Y., Feng, Y., Cheng, M., Zhang, Y., Cai, J., Chen, F.,  
866 Qiu, Y., Jiang, Z., Li, J., Zhang, G., and Mo, Y.: Emission factors and light absorption properties of brown carbon  
867 from household coal combustion in China, *Atmos. Chem. Phys.*, 17, 4769-4780, 10.5194/acp-17-4769-2017, 2017.

868 Tang, J., Li, J., Mo, Y., Safaei Khorram, M., Chen, Y., Tang, J., Zhang, Y., Song, J., and Zhang, G.: Light  
869 absorption and emissions inventory of humic-like substances from simulated rainforest biomass burning in  
870 Southeast Asia, *Environmental Pollution*, 262, 114266, <https://doi.org/10.1016/j.envpol.2020.114266>, 2020.

871 Wang, D., Shen, Z., Zhang, Q., Lei, Y., Zhang, T., Huang, S., Sun, J., Xu, H., and Cao, J.: Winter brown carbon  
872 over six of China's megacities: light absorption, molecular characterization, and improved source apportionment  
873 revealed by multilayer perceptron neural network, *Atmospheric Chemistry and Physics*, 22, 14893-14904,  
874 10.5194/acp-22-14893-2022, 2022a.

875 Wang, Q. Q., Zhou, Y. Y., Ma, N., Zhu, Y., Zhao, X. C., Zhu, S. W., Tao, J. C., Hong, J., Wu, W. J., Cheng, Y. F.,  
876 and Su, H.: Review of brown carbon aerosols in China: Pollution level, optical properties, and emissions, *Journal of*  
877 *Geophysical Research: Atmospheres*, 127, 10.1029/2021JD035473, 2022b.

878 Wang, Y., Pavuluri, C. M., Fu, P., Li, P., Dong, Z., Xu, Z., Ren, H., Fan, Y., Li, L., Zhang, Y.-L., and Liu, C.-Q.:  
879 Characterization of Secondary Organic Aerosol Tracers over Tianjin, North China during Summer to Autumn, *ACS*  
880 *Earth and Space Chemistry*, 3, 2339-2352, 10.1021/acsearthspacechem.9b00170, 2019.

881 Wen, H., Zhou, Y., Xu, X., Wang, T., Chen, Q., Chen, Q., Li, W., Wang, Z., Huang, Z., Zhou, T., Shi, J., Bi, J., Ji,  
882 M., and Wang, X.: Water-soluble brown carbon in atmospheric aerosols along the transport pathway of Asian dust:  
883 Optical properties, chemical compositions, and potential sources, *Science of the Total Environment*, 789, 147971,  
884 10.1016/j.scitotenv.2021.147971, 2021.

885 Wu, G., Fu, P., Ram, K., Song, J., Chen, Q., Kawamura, K., Wan, X., Kang, S., Wang, X., Laskin, A., and Cong, Z.:  
886 Fluorescence characteristics of water-soluble organic carbon in atmospheric aerosol, *Environmental Pollution*, 268,  
887 115906, 10.1016/j.envpol.2020.115906, 2021a.

888 Wu, G. M., Fu, P. Q., Ram, K., Song, J. Z., Chen, Q. C., Kawamura, K., Wan, X., Kang, S. C., Wang, X. P., Laskin,  
889 A., and Cong, Z. Y.: Fluorescence characteristics of water-soluble organic carbon in atmospheric aerosol, *Environ*  
890 *Pollut*, 268, ARTN 115906  
891 10.1016/j.envpol.2020.115906, 2021b.

892 Xie, X., Chen, Y., Nie, D., Liu, Y., Liu, Y., Lei, R., Zhao, X., Li, H., and Ge, X.: Light-absorbing and fluorescent  
893 properties of atmospheric brown carbon: A case study in Nanjing, China, *Chemosphere*, 251, 126350,  
894 10.1016/j.chemosphere.2020.126350, 2020.

895 Yan, J., Wang, X., Gong, P., Wang, C., and Cong, Z.: Review of brown carbon aerosols: Recent progress and  
896 perspectives, *Sci Total Environ*, 634, 1475-1485, 10.1016/j.scitotenv.2018.04.083, 2018.

897 Yu, H., Liang, H., Qu, F., Han, Z. S., Shao, S., Chang, H., and Li, G.: Impact of dataset diversity on accuracy and  
898 sensitivity of parallel factor analysis model of dissolved organic matter fluorescence excitation-emission matrix,  
899 *Scientific Reports*, 5, 10207, 10.1038/srep10207, 2015.

900 Yue, S., Zhu, J., Chen, S., Xie, Q., Li, W., Li, L., Ren, H., Sihui, S., Ping, L., Ma, H., Fan, Y., Cheng, B., Wu, L.,  
901 Deng, J., Hu, W., Ren, L., Lianfang, W., Zhao, W., Tian, Y., and Fu, P.: Brown carbon from biomass burning  
902 imposes strong circum-Arctic warming, *One Earth*, 5, 293-304, 10.1016/j.oneear.2022.02.006, 2022.

903 Yue, S. Y., Bikkina, S., Gao, M., Barrie, L., Kawamura, K., and Fu, P. Q.: Sources and Radiative Absorption of  
904 Water-Soluble Brown Carbon in the High Arctic Atmosphere, *Geophys Res Lett*, 46, 14881-14891,  
905 10.1029/2019gl085318, 2019.

906 Zhan, Y., Li, J., Tsona, N. T., Chen, B., Yan, C., George, C., and Du, L.: Seasonal variation of water-soluble brown  
907 carbon in Qingdao, China: Impacts from marine and terrestrial emissions, *Environmental Research*, 212, 113144,  
908 <https://doi.org/10.1016/j.envres.2022.113144>, 2022.

909 Zhang, Q., Jimenez, J. L., Canagaratna, M. R., Ulbrich, I. M., Ng, N. L., Worsnop, D. R., and Sun, Y.:  
910 Understanding atmospheric organic aerosols via factor analysis of aerosol mass spectrometry: a review, *Analytical*  
911 *Chemistry and Bioanalytical Chemistry*, 401, 3045-3067, 10.1007/s00216-011-5355-y, 2011.  
912 Zhang, Q., Shen, Z., Zhang, T., Kong, S., Lei, Y., Wang, Q., Tao, J., Zhang, R., Wei, P., Wei, C., Cui, S., Cheng, T.,  
913 Ho, S. S. H., Li, Z., Xu, H., and Cao, J.: Spatial distribution and sources of winter black carbon and brown carbon in  
914 six Chinese megacities, *Science of The Total Environment*, 762, 143075,  
915 <https://doi.org/10.1016/j.scitotenv.2020.143075>, 2021.  
916 Zhong, M., and Jang, M.: Light absorption coefficient measurement of SOA using a UV–Visible spectrometer  
917 connected with an integrating sphere, *Atmospheric Environment*, 45, 4263-4271, 10.1016/j.atmosenv.2011.04.082,  
918 2011.  
919 Zhu, C. S., Cao, J. J., Huang, R. J., Shen, Z. X., Wang, Q. Y., and Zhang, N. N.: Light absorption properties of  
920 brown carbon over the southeastern Tibetan Plateau, *Science of the Total Environment*, 625, 246-251,  
921 10.1016/j.scitotenv.2017.12.183, 2018.  
922